Jurassic to Early Cretaceous basin configuration(s) in the Fingerdjupet Subbasin, SW Barents Sea

Christopher Sæbø Serck [a,*], Jan Inge Faleide [a,b], Alvar Braathen [a], Bent Kjølhamar [c], Alejandro Escalona [d]

[a] Department of Geosciences, University of Oslo, P.O. Box 1047, Blindern, 0316 Oslo, Norway
[b] The Center for Earth Evolution and Dynamics, University of Oslo, P.O. Box 1028 Blindern, 0315 Oslo, Norway
[c] TGS, Lensmannslia 4, 1386 Asker, Norway
[d] Department of Petroleum Engineering, University of Stavanger, 4036 Stavanger, Norway

[*] Corresponding author: *E-mail address: c.s.serck@geo.uio.no*

Key words:

Tectonics
Fingerdjupet Subbasin
Barents Sea
Extensional faulting events
Growth packages

Abstract

The Fingerdjupet Subbasin in the southwestern Barents Sea sits in a key tectonic location between deep rifts in the west and more stable platform areas in the east. Its evolution is characterized by extensional reactivation of N-S and NNE-SSW faults with an older history of Late Permian and likely Carboniferous activity superimposed on Caledonian fabrics. Reactivations in the listric NNE-SSW Terningen Fault Complex accommodated a semi-regional rollover structure where the Fingerdjupet Subbasin developed in the hangingwall. In parallel, the Randi Fault Set developed from outer-arc extension and collapse of the rollover anticline.

N-S to NNE-SSW faults and the presence of other fault trends indicate changes in the stress regime relating to tectonic activity in the North Atlantic and Arctic regions. A latest Triassic to Middle Jurassic extensional faulting event with E-W striking faults is linked to activity in the Hammerfest Basin. Cessation of extensional tectonics before the Late Jurassic in the Fingerdjupet Subbasin, however, suggests rifting became localized to the Hammerfest Basin. The Late Jurassic was a period of tectonic quiescence in the Fingerdjupet Subbasin before latest Jurassic to Hauterivian extensional faulting, which reactivated N-S and NNE-SSW faults. Barremian SE-prograding clinoforms filled the relief generated during this event before reaching the Bjarmeland Platform. High-angle NW-prograding clinoforms on the western Bjarmeland Platform are linked to Early Barremian uplift of the Loppa High. The Terningen Fault Complex and Randi Fault Set were again reactivated in the Aptian along with other major fault complexes in the SW Barents Sea, leading to subaerial exposure of local highs. This activity ceased by early Albian. Post-upper Albian strata were removed by late Cenozoic uplift and erosion, but later tectonic activity has both reactivated E-W and N-S/NNE-SSW faults and also established a NW-SE trend.

1. Introduction

The Fingerdjupet Subbasin of the southwestern Barents Sea has thick Jurassic to Lower Cretaceous deposits buried relatively shallow in the present day subsurface (Figs. 1, 2). This contrasts both the Bjarmeland Platform to the east, where late Cenozoic uplift and erosion has removed much of the Lower Cretaceous section, and the Bjørnøya Basin to the west, where present burial depth makes high-resolution seismic imaging of these deposits challenging. The Fingerdjupet Subbasin therefore has a cornerstone position in this part of the southwestern Barents Sea, and may provide valuable insights into the Jurassic to Early Cretaceous evolution of not only the study area, but of the whole region.

Previous workers have described extensional faulting in the Fingerdjupet Subbasin (e.g. Rønnevik & Jacobsen, 1984; Gabrielsen et al., 1990; Faleide et al., 1993a, 1993b; Gudlaugsson et al., 1998), but data coverage and resolution has not allowed for a detailed analysis of the timing of extensional faulting events. For this study we utilize a large, high-resolution 3D dataset together with information from nearby hydrocarbon exploration wells (7321/7-1, 7321/8-1 and 7321/9-1; Fig. 3) and a shallow stratigraphic borehole (7320/3-U-1). The 3D dataset allows for semi-regional horizon and fault mapping and can be considered the outline of the study area (Fig. 1). Timing of extensional faulting episodes displayed by sedimentary growth packages is examined in local depocenters, where seismic and stratigraphic resolution is at the highest possible level.

We recognize the seismic dataset holds great potential for investigation of sedimentary deposits and associated fault systems from pre-Carboniferous to recent, and some considerations around basin history prior to the latest Triassic have been made. The aim of the current study, however, is to establish a detailed seismic- and tectonostratigraphic framework for the Jurassic to Lower Cretaceous deposits of the Fingerdjupet Subbasin.

2. Geological framework

The present day Barents shelf is located at the northwestern corner of the Eurasian plate (Fig. 1a) (Faleide et al., 2008). The geological evolution of the area is characterized by a series of compressional and later extensional events related to continent assembly and breakup, respectively (e.g. Faleide et al. 1993b, 1996; Gudlaugsson et al., 1998). The southwestern Barents Sea consists of a complex pattern of basins and highs which strikes predominantly NE-SW and N-S (Fig. 1b) (Faleide et al., 1993b; Gudlaugsson et al., 1998). The Fingerdjupet Subbasin (Fig. 1c) was defined as the shallow, northeastern part of the Bjørnøya Basin by Gabrielsen et al. (1990).

2.1 Post-Caledonian extensional faulting

The study area has been affected by at least five post-Caledonian phases of extensional faulting: Late Devonian orogenic collapse, mid-late Carboniferous extensional faulting, Late Permian to Early Triassic extensional faulting focused in the west, Middle Jurassic-Early Cretaceous extensional faulting and Late Cretaceous-Cenozoic rifting (Gudlaugsson et al., 1998; Faleide et al., 1993b, 2015; Glørstad-Clark, 2011). While the post-Caledonian evolution of the SW Barents Sea has been dominated by these extensional events, some inversion of major fault complexes have also previously been described (e.g. Faleide et al., 2008; Gabrielsen et al., 1997; Indrevær et al., 2016).

The study area is most likely underlain by Caledonian basement (Gernigon and Brönner, 2012; Ritzmann and Faleide, 2007) that was assembled by thrusting during the Caledonian Orogeny when Laurentia and Baltica collided in the Silurian to Early Devonian (Doré, 1991). A Caledonian terrain affected by collapse has been inferred both in the SW Barents Sea, mainly based on magnetic data (Gernigon and Brönner, 2012), and further north between Bjørnøya

and Svalbard (Breivik et al., 2003; Gudlaugsson and Faleide, 1994; Ritzmann and Faleide, 2007). N to NNW trends seen in magnetic data in the area between Svalbard and the Loppa High are believed to represent the structural grain of Caledonian thrusting (Barrère et al., 2009; Gernigon et al., 2014; Gernigon and Brönner, 2012). On Bjørnøya, Braathen et al. (1999b) provided evidence for WNW-directed Caledonian thrusting and Carboniferous extensional reactivation of these contractional structures, and Worsley et al., (2001) subsequently documented Carboniferous syntectonic deposits along mainly N-S striking normal faults. Gernigon et al. (2014) described a major NW-dipping detachment along the northern flank of the Stappen High and SW-to-W-dipping detachments in the Bjørnøya Basin, while Gudlaugsson et al. (1998) described an E-dipping detachment in the Fingerdjupet Subbasin (Fig. 2). To explain this complexity, Gernigon et al. (2014) suggested an accommodation or relay zone between major detachments exist between the Loppa and Stappen highs.

In mid-Carboniferous to Late Carboniferous times, a 300 km wide and at least 600 km long zone of rifting developed in the Barents Sea, resulting in a series of extensional basins separated by fault-bounded highs, e.g. the Nordkapp, Maud, Bjørnøya, Ottar and Tromsø basins (Faleide et al., 2015; Gudlaugsson et al., 1998) (Fig. 1b). The Carboniferous rift structures, mainly with a clastic basin fill but also some evaporites, are capped by a regional carbonate platform that developed during latest Carboniferous-early Permian times (e.g. Faleide et al., 2015; Henriksen et al., 2011b; Larssen et al., 2002). It has been suggested that the Bjørnøya Basin and Fingerdjupet Subbasin formed as rift basins initiated in mid-Carboniferous times (Dengo and Røssland, 1992; Gudlaugsson et al., 1998). For the Bjørnøya Basin, this suggestion is supported by the presence of salt diapirs as indicated by Breivik et al. (1998) and better constrained in recently acquired seismic and potential field data. Investigations from the northern Bjørnøya Basin and southern Stappen High by Blaich et al. (2017) also indicate mid-Carboniferous rifting with deposition of growth packages along NE-SW striking faults.

The western parts of the Barents Sea experienced another phase of extension in the Late Permian to Early Triassic (Gudlaugsson et al., 1998). Recently, improved seismic imaging has allowed interpretation of growth packages of this age in the Bjørnøya Basin, Fingerdjupet Subbasin and southern Stappen High (Blaich et al., 2017; Faleide et al., 2015; Glørstad-Clark, 2011; Kamp, 2016). A distinct growth sequence in the Bjørnøya Basin along the Leirdjupet Fault Complex can be tied to a similar unit in the Fingerdjupet Subbasin, where age control is provided by well 7321/8-1 ("Norwegian Petroleum Directorate Factpages," 2017).

The underfilled epicontinental basin that existed in the Barents Sea area in the Early Triassic was gradually infilled by W-NW prograding clastic wedges from earliest-Middle Triassic (Glørstad-Clark et al., 2010). The Fingerdjupet Subbasin persisted as an underfilled depocenter throughout the Early-Middle Triassic but was filled by fluvio-deltaic deposits in the Late Triassic (Glørstad-Clark et al., 2010; Kamp, 2016). Kamp (2016) described growth packages within Upper Triassic strata linked to N to NNE striking faults in the Fingerdjupet Subbasin, thus suggesting a Late Triassic extensional faulting event. Osmundsen et al. (2014) described fault-controlled sedimentary architecture relating to E-W to NW-SE striking normal faults in the Tschermakfjellet and De Geerdalen formations on Edgeøya (Carnian and Carnian to early Norian, respectively) and Flatsalen Formation (Norian) on Hopen (Fig.1). Mulrooney et al. (2017) suggested Mesozoic extensional faulting along crudely E-W striking faults in the Goliat area of the Hammerfest Basin started in the Norian.

The Middle to Late Jurassic was a period of regional extension, resulting in a regional rift basin extending from the Rockall Trough west of Ireland to the Barents Sea (Faleide et al., 1993b). The structuring of the southwestern Barents Sea from the late Middle Jurassic to earliest Cretaceous was closely affiliated with both the North Atlantic and Arctic regions, represented by

147 the rifting in the North Atlantic and Amerasia basins, respectively (Faleide et al., 1993b).
148 Mesozoic rifting in the Hammerfest Basin culminated with a Late Jurassic to earliest Cretaceous
149 rift event which also affected the Bjørnøya Basin and southern Stappen High, reactivating the
150 pre-existing tectonic grain (Blaich et al., 2017; Faleide et al., 1993b). Extensional faulting on E-
151 W striking faults in the Hammerfest Basin had ceased by early Barremian times, when the
152 Loppa High was uplifted, causing inversion in normal fault complexes along its flanks (Indrevær
153 et al., 2013).
154 Faleide et al. (1993a) attributed the N-S to NNE-SSW horst and graben pattern of the
155 Fingerdjupet Subbasin to Late Jurassic rifting with later local reactivation. North Atlantic
156 tectonism appears to dominate increasingly through the Early Cretaceous, and major extension
157 along the western Barents Sea margin led to the formation and/or rejuvenation of several fault
158 complexes such as the Troms-Finnmark Fault Complex, Ringvassøy-Loppa Fault Complex,
159 Bjørnøyrenna Fault Complex and Leirdjupet Fault Complex, and rapid subsidence of the
160 adjacent Harstad, Tromsø and Bjørnøya basins (Faleide et al., 1993b). The Leirdjupet Fault
161 Complex, which separates the deep Bjørnøya Basin from the shallower Fingerdjupet Subbasin,
162 was active at this time, and both erosional truncation of intra-basinal highs and growth packages
163 banked onto the fault have previously been described (Faleide et al., 1993b). Faleide et al.
164 (1993b) recognized Berriasian/Valanginian and Hauterivian/Barremian phases of extension in
165 the western Hammerfest Basin but were unable to resolve them on seismic data. Although an
166 extensional regime prevailed in the SW Barents for the better part of the Early Cretaceous, early
167 Barremian uplift of the Loppa High caused inversion in the surrounding fault complexes and led
168 to subaerial exposure of the Loppa High (Indrevær et al., 2016).
169
170 Magmatism within the High Arctic Large Igneous Province (HALIP, ~125 Ma), likely related to
171 the rifting, breakup and early stage of seafloor spreading in the Amerasia Basin, is suggested to
172 have caused regional uplift of the northern Barents margin and adjacent areas of the proto-

Arctic (e.g. Senger et al., 2014). In the Barremian and Aptian, large volumes of sediments were shed from the uplifted region, allowing large fluvio-deltaic complexes to prograde southeastwards past Svalbard to the southwestern Barents Sea area (Faleide et al., 1993b; Midtkandal & Nystuen, 2009; Faleide et al., 2015; Marín et al., 2016). Lower Cretaceous intrusive and extrusive igneous rocks are found throughout the Barents Sea (Polteau et al., 2016), but so far not documented in the southwestern Barents Sea. The igneous activity has been dated to 122-124 Ma based on samples from Svalbard and Franz Josef Land (Corfu et al., 2013). Based on field-, seismic- and potential field data, magmatism on the Barents shelf E and SE of Svalbard display a NNE trend (Grogan et al., 2000; Minakov et al., 2012).

Mesozoic extension along the western Barents Sea margin affecting the Bjørnøya, Harstad and Tromsø basins peaked in the Aptian (Faleide et al., 1993b). This is supported by improved seismic imaging and interpretation of the northern Bjørnøya Basin and southern Stappen High (Blaich et al., 2017). The Bjørnøya Basin, which was faulted along NNE-SSW and N-S faults, experienced rapid subsidence and infill also after the cessation of faulting (Faleide et al., 1993a, 1993b). The Hammerfest Basin not only experienced extension in faults along the E-W basin axis, but also saw an increased influence of North Atlantic tectonic activity as evident by normal faulting in the N-S trending Ringvassøy-Loppa Fault Complex (Faleide et al., 1993b).

In the Late Cretaceous and Paleogene the Barents Sea area was affected by another phase of extension which culminated with breakup and seafloor spreading in the Norwegian-Greenland Sea in the earliest Eocene (Faleide et al., 2008). Narrow basins in the SW Barents Sea (e.g. Sørvestsnaget Basin) (Faleide et al., 2008) and NE Greenland (Wandel Sea Basin) (Svennevig et al., 2017) developed within the so-called De Geer Zone in response to regional shear. The Cenozoic western Barents Sea continental margin is characterized by transform faulting in the south, represented by the Senja Fracture Zone, and a rifted segment located southwest of

Bjørnøya where extensive volcanism has occurred in the Vestbakken Volcanic Province (Faleide et al., 2008). Further north, there is an initially sheared and later rifted margin along the Hornsund Fault Zone (Faleide et al., 2008). Some fault complexes in the western Barents Sea experienced periods of inversion in the Late Cretaceous and Paleogene, likely relating to transpression along sheared margin segments (e.g. Faleide et al., 2015, 2008; Braathen et al., 1999a; Gabrielsen et al., 1997; Indrevær et al., 2016; Vågnes et al., 1998).

2.2 Late Cenozoic uplift and erosion

The entire Barents Shelf was uplifted and eroded during the Neogene (Baig et al., 2016; Henriksen et al., 2011a). A significant part of the erosion, and deposition of large volumes of Plio-Pleistocene glacial sediments along the continental margins in the west and north (Dimakis et al., 1998; Faleide et al., 1996; Laberg et al., 2012), was related to the northern hemisphere glaciations, but uplift of large areas was initiated earlier (Oligocene?-Miocene) due to other tectonic causes (Dimakis et al., 1998). Post-Early Cretaceous strata were removed from the Fingerdjupet Subbasin (Faleide et al., 1996; Henriksen et al., 2011). The uplift and associated erosion was greater north of the Fingerdjupet Subbasin, making correlation of the Cretaceous sedimentary succession between Svalbard and the southwestern Barents Sea challenging. The net erosion in the Fingerdjupet Subbasin varies from approximately 1600 m in the south to 2600 m in the north (Henriksen et al., 2011; Baig et al., 2016). The boundary between pre-glacial rocks and Quaternary glacial deposits is marked by the upper regional unconformity (URU) (Solheim and Kristoffersen, 1984).

3. Datasets and methods

Key to this study is an 8600 km^2 3D seismic survey which was acquired by TGS in 2013 utilizing ten 6000 m long seismic streamers with a streamer separation of 75 m and an E-W acquisition direction. 3D seismic bin size is 18.75 m x 6.25 m and the dataset extends to 7000 ms TWT. The data is zero-phased with SEG (Society of Exploration Geophysicists) positive standard polarity, where positive amplitudes correspond to an increase in acoustic impedance across an interface. In addition, regional 2D seismic lines acquired by TGS and Fugro between 2006 and 2012 have been used to examine the Fingerdjupet Subbasin in a regional context.

The geometrical characteristics of the seismic packages have been examined through a combination of horizon- and fault mapping (e.g. Figs. 1 and 2). In total 16 horizons have been mapped to investigate the basin architecture. In addition to conventional fault mapping on seismic sections, seismic variance attribute has been draped on the interpreted seismic horizons to illustrate how different parts of the sedimentary succession have been affected by different fault systems. Time-thickness maps produced from the interpreted horizons have been used to highlight and assess variations related to sedimentary systems and/or geometry of sedimentary sinks. Three hydrocarbon exploration wells have been drilled in the Fingerdjupet Subbasin but south of the 3D seismic dataset used for this study, penetrating Lower Cretaceous to Upper Permian stratigraphy. Checkshot data from wells 7321/7-1, 7321/8-1 and 7321/9-1 (Fig. 1), located between 7.5 km and 25 km south of the 3D seismic dataset, give average seismic velocities between ca. 2800 and 4100 m/s for the Lower Cretaceous to Upper Triassic stratigraphy of the Fingerdjupet Subbasin (Table 1). These calculations are used to convert fault throw and thickness of seismic packages from milliseconds Two Way Traveltime [ms TWT] to metres [m]. The maximum frequency of the dominant bandwidth varies with depth, and estimates for seismic resolution for the Upper Triassic, Jurassic and Cretaceous strata are given in Table 2.

In addition, 10 of the 16 interpreted horizons have been correlated with publicly available biostratigraphic and petrophysical data from well 7321/7-1 (Robertson Group, 1989) (Fig. 4). This has allowed for establishing a seismic stratigraphic and tectonostratigraphic framework for the study area (Fig. 5). Time-thickness maps and corresponding seismic profiles for the sequences are given in Fig. 6. The horizon names reflect the ages of the horizons as inferred from the biostratigraphy report (Robertson Group, 1989). Not all the ages inferred from the biostratigraphy report are based on direct biostratigraphic evidence taken from sidewall cores. Some ages are based on petrophysical log analysis from the well coupled with regional well information, often aided by biostratigraphic evidence above and below. Gamma ray logs as sand/clay indicators are used to gain a brief overview of the depositional setting of lithological groups in the Fingerdjupet Subbasin (Fig. 3), and to support age determination where biostratigraphic evidence is scarce (Fig. 4) (Robertson Group, 1989).

In the 1980's and 1990's, IKU (Continental Shelf Institute, now SINTEF Petroleum Research) drilled a number of shallow stratigraphic boreholes near the main study area. Of particular interest is borehole 7320/3-U-1, which is located within the limits of the 3D seismic survey used for this study (Fig. 1). This 36,2 m core contains Barremian to Tithonian strata with a 3 m thick condensed section of Valanginian age, and thus may provide a data point that can be tied to the available 3D seismic coverage (Århus et al., 1990). Due to constraints in seismic resolution, however, a direct tie remains challenging.

Three new structural elements have been defined (Appendix) and approved by the Norwegian Committee on Stratigraphy (NSK); these are the Ringsel Ridge, Terningen Fault Complex and Randi Fault Set.

4. Fault systems of the Fingerdjupet Subbasin

Fault systems observed in the study area affect different stratigraphic intervals and vary significantly in terms of orientation, geometry and displacement. The main fault trends are NNE-SSW, N-S, E-W and NW-SE. NNE-SSW and N-S faults commonly have a strong affiliation with wedge-shaped seismic packages in the hangingwall and are seen as boundary faults to the Bjørnøya Basin and Fingerdjupet Subbasin (Figs. 1, 2, 6, 7, 8). Most faults shown in Fig. 2 have this trend and some are considered significant enough to be given names. These are the Terningen Fault Complex, which defines the western boundary of the Fingerdjupet Subbasin, and the Randi Fault Set, which is seen as densely spaced faults straddling the transition between the Fingerdjupet Subbasin and the Bjarmeland Platform. In the Randi Fault Set, the Bjarmeland Platform rolls over from sub-horizontal to westwards dipping reflectors into the Terningen Fault Complex (Fig. 2). Together, the Leirdjupet and Terningen fault complexes define the Ringsel Ridge.

4.1 NNE-SSW faults

A prominent system of normal faults striking approximately NNE-SSW dominates the study area (Fig. 1). The Ringsel Ridge separates the Bjørnøya Basin from the Fingerdjupet Subbasin and is bounded to the west by the Leirdjupet Fault Complex and to the east by large, east-facing NNE-SSW and N-S oriented normal faults in the Terningen Fault Complex (Figs. 1, 2, 7, 8). NNE-SSW oriented faults are also observed in the Bjørnøya Basin to the west and in the Hoop Fault Complex and Maud Basin to the east. Faults are planar for the Mesozoic level but some, for instance faults in the Terningen Fault Complex, have a listric expression at depth, where the interpreted fault surface curves into a lower-angle surface at approximately 5 s TWT (Fig. 2, stippled line).

The easternmost fault in the Terningen Fault Complex forms the boundary between the main Lower Cretaceous Fingerdjupet depocenter and the Ringsel Ridge. This fault consists of two main segments where the southern segment is oriented N-S and the northern segment is oriented NNE-SSW (Fig. 1). Maximum displacement of the Berriasian-Tithonian horizon by 600 ms TWT (ca. 830 m) to 700 ms TWT (ca. 970 m) in the Fingerdjupet Subbasin is observed where the two fault segments branch. In the Randi Fault Set, fault displacement is generally smaller than 250 ms TWT (ca. 350 m) (Figs. 2 and 7). NNE-SSW faults defining large fault blocks in the Bjørnøya Basin displace the Berriasian-Tithonian by between 500 and 600 ms TWT (ca. 700-830 m) (Fig. 1c). The NNE-SSW fault segments truncating the Berriasian-Tithonian horizon are straight to slightly curved. There are, however, some en echelon fault segments with various degree of linkage, from soft-links via relay ramps to hard-links (Fig. 1c, north of the Terningen Fault Complex).

The large west-facing NNE-SSW faults in the Bjørnøya Basin define the boundaries between large rotated fault blocks (Figs. 1 and 2). Stratigraphy of Carboniferous or older to Early Cretaceous age is affected by NNE-SSW faults in the Bjørnøya Basin and Fingerdjupet Subbasin (Fig. 2). The faults are occasionally truncated by the Upper Regional Unconformity (Base Quaternary).

Wedge-shaped seismic packages thickening towards faults trending NNE-SSW can be observed between several interpreted stratigraphic surfaces in the study area: Intra Permian to Middle Triassic (Fig. 2), Berriasian-Tithonian to intra upper Hauterivian (Fig. 6, Sequence 3) and intra Barremian to intra lower Albian (Fig. 6, Sequence 5). The Lower Cretaceous wedges can be seen in seismic sections in Figures 7 and 8. Along strike of the Terningen Fault Complex, local transverse folds are observed between the Berriasian-Tithonian and intra lower Albian horizons (Fig. 9). These anticlines and synclines with fold axis orthogonal to fault strike suggest fault displacement maxima and minima related to relay zones (Fig. 9).

4.2 N-S faults

The large west-facing Leirdjupet Fault Complex, defining the eastern boundary of the Bjørnøya Basin and western boundary of the Ringsel Ridge, is one of few but prominent N-S striking extensional fault arrays in the study area. As seen in Fig. 1, this fault complex link up with a large NNE-SSW fault west of the shallow stratigraphic borehole 7320/3-U-1 via a number of en echelon fault segments striking approximately NNW-SSE. Vertical displacement of the Berriasian-Tithonian horizon over the Leirdjupet Fault Complex decreases from approximately 2500 ms TWT (ca. 3470 m) in the southern part of the study area to less than 190 ms TWT (ca. 260 m) 60 km farther north. Fault activity is displayed by several Lower Cretaceous wedge-shaped packages in the Bjørnøya Basin, which thicken towards the Leirdjupet Fault Complex (Figs. 2 and 8).

4.3 E-W faults

A fault population striking approximately E-W is observed throughout the study area (Fig. 1c). Compared to the previously described fault systems, fault displacements of the Berriasian-Tithonian horizon are relatively modest, commonly in the range of 10-100 ms TWT (ca. 10-140 m) but locally up to 180 ms TWT (ca. 250 m). For the Berriasian-Tithonian horizon, individual faults are straight and can be traced along strike for up to 25 km. In the Fingerdjupet Subbasin and the eastern Bjarmeland Platform the displacement is for the most part less than 100 ms TWT (ca. 140 m), affecting Upper Triassic to Lower Cretaceous stratigraphy. The E-W oriented faults generally tip out down section in the lower part of the Upper Triassic interval. Minor growth packages towards E-W oriented faults are observed between the intra lower Norian and

Oxfordian-Callovian horizons (Fig. 6, Sequence 1). The E-W oriented faults have also been active at a later stage, as indicated by fault displacements of the lower-middle Albian and upper Albian surfaces (Fig. 10). With faults mostly truncated at the URU, and absence of associated growth wedges in the preserved Lower Cretaceous section, dating of this fault activity is difficult. However, it certainly post-dates the early Albian.

4.4 NW-SE faults

An extensive system of NW-SE striking faults is observed in the 3D dataset. The fault system can be seen in seismic sections in Figs. 7 and 8 and in variance attribute maps for the lower-middle Albian and upper Albian horizons in Fig. 10. Maximum displacement is seen near the intra Lower Albian and lower-middle Albian horizons. Fault displacement varies from approximately 25 ms TWT (ca. 40 m) to near seismic resolution (17 - 10 m; Table 2) for the lower-middle Albian horizon. In seismic sections, the fault plane characteristics vary from virtually transparent to strongly reflective, with reflective faults traceable across the Fingerdjupet Subbasin. Timing of the fault activity is problematic as no growth wedges are observed and many faults are truncated at the URU. Figure 10b shows how the upper Albian horizon, which is the uppermost interpretable Lower Cretaceous horizon in the Fingerdjupet Subbasin, is affected by the NW-SE fault system. The largest vertical displacements are seen near the intra lower Albian to lower-middle Albian horizons and the faults either tip out in the lower Albian or Aptian, or they interfere with the upper fault tips of deeper-seated faults, sometimes resulting in a significantly higher fault density such as above NNE-SSW faults in the Randi Fault Set (Fig. 7). Fault interaction is indicated by curved fault intersections with mainly E-W faults but also with the upper part of the Terningen Fault Complex (Fig. 10).

5. Basin architecture

The Upper Triassic to recent strata present in the Fingerdjupet Subbasin have been divided into seven sequences. Results from the seismic interpretation are shown on seismic sections in Figs. 2, 6, 7 and 8, and as a time-structure map for the Berriasian-Tithonian horizon in Fig. 1. Fig. 5 presents a summary of the mapped seismic horizons and how they relate to chronostratigraphy, observed seismic geometries and thereby sequences. An overview of thickness variations for Sequences 1, 2, 3, 4, 5A and 5B is presented in Fig. 6. Wedge-shaped seismic geometries pre-dating the Late Triassic are clearly seen in the Bjørnøya Basin and Fingerdjupet Subbasin in Fig. 2, however, detailed description of these is beyond the scope of this work; information is given in Kamp (2016). Lower to Middle Triassic deltaic deposits have a substantial thickness in the Hoop Fault Complex but pinch out or condense rapidly W towards the Fingerdjupet Subbasin (Fig. 2).

5.1. Sequence 1: Intra lower Norian to Oxfordian-Callovian (iln-OC)

Sequence 1 shows a general westward increase in thickness, from 40 to 120 ms TWT (ca. 70 - 200 m). The thickest part of the sequence is seen on the Ringsel Ridge (Figs. 7 and 8). In the Fingerdjupet Subbasin, smaller-scale time-thickness variations are observed as wedge-shaped seismic packages with 20 to 30 ms TWT (ca. 30 - 50 m) thickness increase towards E-W oriented faults (Fig. 6, Sequence 1). In the northern part of the study area, the sequence locally increases in thickness towards the top of the footwall blocks of faults oriented NNE-SSW.

5.2 Sequence 2: Oxfordian-Callovian to Berriasian-Tithonian (OC-BT)

Sequence 2 varies in thickness between 10 and 70 ms TWT (ca. 20 – 120 m). There is a general westwards thickness increase and a small but distinct thickness increase is observed along a smooth, gently curved, northeast to north oriented line through the study area (Fig. 6-

Sequence 2). The sequence does not seem to change thickness neither across faults oriented E-W nor the N-S to NNE-SSW oriented faults in the Terningen Fault Complex.

5.3 Sequence 3: Berriasian-Tithonian to intra upper Hauterivian (BT-iuH)

Sequence 3 is characterized by wedge-shaped seismic packages, where there is a thickness increase towards NNE-SSW striking normal faults (Fig. 6-Sequence 3, Figs. 7 and 8). The thickness varies from approximately 200 ms TWT (ca. 280 m) close to the Terningen Fault Complex to 20 ms TWT (ca. 30 m) along the eastern margin of the basin. Wedge-shaped seismic packages thicken both towards the Terningen Fault Complex and towards faults bounding individual rotated fault blocks within the Fingerdjupet Subbasin and the Randi Fault Set. This fault array with associated sedimentary growth packages is shown in a seismic section in Fig. 7 and in a Berriasian-Tithonian time-structure map in Fig. 1. Sequence 3 reflectors are cut by faults while onlapping the hangingwall dipslopes (Fig. 7). No significant erosion of the footwall highs has been observed. Locally, E-W striking faults appear to have an influence on thickness variation observed in the data as seen in the time-thickness map (Fig. 6, Sequence 3).

5.4 Sequence 4: Intra upper Hauterivian to intra Barremian (iuH-iB)

Sequence 4 varies in thickness from 200 to 500 ms TWT (ca. 280-700 m). In the Ringsel Ridge the top of the sequence has been truncated by the intra Barremian horizon and 200-250 ms TWT thickness (ca. 280 - 350 m) is recorded (Fig. 7). In the Fingerdjupet Subbasin the thickness varies between 350 to 400 ms TWT (ca. 490-560 m). Along the eastern flank of the Fingerdjupet Subbasin the sequence records a time-thickness between 420 and 500 ms TWT (ca. 580-690 m) and on the Bjarmeland Platform in the eastern part of the study area the thickness is 350-400 ms TWT (ca. 490-560 m). The thickness variations of Sequence 4 occur across NNE-SSW and N-S trending faults; mainly for the Terningen Fault Complex but also

across faults with less displacement in the Randi Fault Set. The sequence shows two oppositely directed systems of prograding clinoforms (Figs. 11 and 12). SE prograding clinoforms (Fig. 11) are most easily observed on the platform east in the study area where the succession is relatively flat-lying, the fault density is low and the present burial depth is shallow. This system can also be observed in the Randi Fault Set, where detailed correlation is made difficult by densely spaced NNE-SSW faults, and in the Fingerdjupet Subbasin, although the level of detail is lower than on the Bjarmeland Platform because of the greater burial depth (Fig. 7). In the southeastern part of the study area, on the Bjarmeland Platform, the SE prograding clinoform system merges with and overlies another system of clinoforms displaying a NW direction of progradation and steeper foreset angles (Fig. 12). The clinoform systems are overlain by a conformable succession of laterally continuous, parallel reflections. The top of this succession shows a varying degree of erosional truncation at the intra Barremian horizon.

5.5 Sequence 5: Intra Barremian to intra lower Albian (iB-ilAl)

Sequence 5 shows pronounced wedge-shaped geometries and thickening of seismic packages towards NNE-SSW faults in the study area (Figs. 2, 6-sub-sequences 5A and 5B, 7 and 8). In the most prominent Lower Cretaceous Fingerdjupet depocenters the sequence reaches thicknesses of approximately 600 ms TWT (ca. 830 m), while it thins towards the platform in the east to less than 50 ms TWT (ca. 70 m). From the base to the top of sequence 5 there is a marked change in which faults control the distribution of sediments, as indicated in Fig. 5. Sequence 5 has therefore been divided into two sub-sequences.

5.5.1 Sub-sequence 5A: Intra Barremian to intra Aptian 1 (iB-iA1)

Sub-sequence 5A is characterized by pronounced thickening towards the Terningen Fault Complex and several other smaller faults in the Randi Fault Set, strengthening the half-graben

versus footwall high morphology across the Fingerdjupet Subbasin (Fig. 7). The sub-sequence is not present in the Ringsel Ridge, where the intra Barremian horizon can be seen truncating parts of sequence 4 (Fig. 13b). Sub-sequence 5A onlaps the intra Barremian horizon at individual footwall highs in the Randi Fault Set as well as the eastern margin of the Fingerdjupet Subbasin. The intra lower Aptian horizon (internal to sub-sequence 5A) locally truncate strata of the lower part of sub-sequence 5A east in the Fingerdjupet Subbasin and in the Randi Fault Set (Fig. 13c). Wedge-shaped seismic packages deposited roughly contemporaneously with this sub-sequence are observed in the hangingwall of the Leirdjupet Fault Complex in the Bjørnøya Basin (Figs. 2 and 8). The intra Aptian 1 horizon (base sub-sequence 5B) is the first horizon to blanket both the Ringsel Ridge and the Randi Fault Set (Figs. 7, 8, 13).

5.5.2 Sub-sequence 5B – intra Aptian 1 to intra lower Albian (iA1-ilAl)

Sub-sequence 5B drapes the Randi Fault Set but shows a significant thickening towards the Terningen Fault Complex. Progressively smaller time-thickness differences between the main Fingerdjupet Subbasin depocenter and the adjacent Ringsel Ridge are observed up section (Figs. 7 and 8). In the Ringsel Ridge the thickness of sub-sequence 5B varies between 150-200 ms TWT (ca. 210-280 m) whereas in the Fingerdjupet Subbasin the thickness reaches 300 ms TWT (ca. 420 m).

5.6 Sequence 6: Intra lower Albian to Upper Regional Unconformity (ilAl-URU)

The Albian strata of the Fingerdjupet Subbasin are truncated by the URU. Accordingly, thickness variations of sequence 6 are strongly affected by uplift and erosion, which have removed progressively older strata towards the basin margins (Figs. 7 and 8). The lower parts of sequence 6, from intra lower Albian to lower-middle Albian, are present in most parts of the basin and record a slight, gradual westward thickening. The sequence onlaps the eastern basin

457 margin until Upper Albian strata drape the western Bjarmeland Platform. No thickness variations
458 associated to any fault trends are observed, but the package has been offset by NNE-SSW,
459 NW-SE and E-W oriented fault systems after deposition (Fig. 10).

460 ### 5.7 Sequence 7: Upper Regional Unconformity – seabed (URU-Sb)

461 Sequence 7 consists of Quaternary deposits with common SW-NE oriented iceberg plough
462 marks at the seabed. The lower boundary surface is the URU, which separates the sequence
463 from the underlying Lower Cretaceous deposits. The time-thickness of the sequence varies
464 between approximately 70 ms TWT in the southwest to practically zero in the northwest towards
465 the Stappen High. Seismic sections in Figs. 2, 7 and 8 show the URU eroding deeply into the
466 Albian strata in the Fingerdjupet Subbasin.

467

6. Discussion

We aim at establishing a seismic- and tectonostratigraphic framework for the Jurassic to Lower Cretaceous strata of the Fingerdjupet Subbasin; however, reactivation of previously established tectonic fabrics seems obvious and calls for a short discussion on inheritance and larger-scale structure. The results presented in chapters 4 and 5 are subsequently discussed in a western Barents Sea context to assess the regional significance of observations from the Fingerdjupet Subbasin.

6.1 Local inheritance and reactivation

The Terningen Fault Complex is a fundamental structure that controls accommodation space creation in the Fingerdjupet Subbasin. Sedimentary growth packages suggest deposition during periods of active extensional faulting as illustrated in Figures 5, 6, 7 and 8. On a large scale, the Fingerdjupet Subbasin can be seen as a semi-regional rollover structure where the Bjarmeland Platform rolls into the Terningen Fault Complex. Extension is accommodated by displacement on the Terningen Fault Complex that changes/link into an underlying lower-angle detachment fault at depth (Fig. 2, ~5 s TWT). This seismically mappable fault geometry gives a listric expression that offers a viable explanation for the overlying rollover fold (e.g. Hongbin Xiao and Suppe, 1992). Closely spaced sub-parallel faults in the Randi Fault Set may either represent breakdown faults in the rollover, with antithetic and synthetic faults rooted in the deeper detachment, or outer-arc extension faults in the rollover anticline (Figs. 1c, 2). Extensional faults in the crest of rollover anticlines have been demonstrated on a variety of scales from seismic data to analogue experiments (e.g. Hongbin Xiao and Suppe, 1992; Mauduit and Brun, 1998; McClay, 1990).

Extensional faulting likely reactivated the underlying structural grain of Caledonian contractional structures (Barrère et al., 2009; Blaich et al., 2017; Gernigon et al., 2014; Gernigon and Brönner, 2012; Ritzmann and Faleide, 2007), which has been described on Bjørnøya by

493 Braathen et al. (1999b) and Worsley et al. (2001). There, Caledonian thrusts were reactivated
494 as normal faults in the Carboniferous, resulting in syn-tectonic deposition mainly related to N-S
495 striking faults. Blaich et al. (2017) mapped mid-Carboniferous growth packages linked to NE-
496 SW striking faults in the northern Bjørnøya Basin and southern Stappen High. Wedge-shaped
497 seismic packages of pre-Permian age have not, however, been observed in the Fingerdjupet
498 Subbasin. Although beyond the scope of this work, it is worth noting that syn-extensional
499 deposits related to low-angle detachment faults might display different geometries than the
500 typical wedge-shaped seismic geometries related to steeply dipping normal faults (Friedmann
501 and Burbank, 1995; Peron-Pinvidic et al., 2007). Hence, Carboniferous (and/or Devonian)
502 extension might have affected the Fingerdjupet Subbasin even though there are no observable
503 growth packages in the assumed pre-Permian stratigraphy. Speculatively, pre-Late-Permian
504 extension in the Fingerdjupet Subbasin may have been accommodated by extensional
505 reactivation of Caledonian thrust faults, perhaps represented by e.g. the proposed low-angle
506 detachment in Figure 2 (~5 s TWT). The steeply dipping Terningen Fault Complex, which has
507 been instrumental for the current basin architecture, was then established in the Late Permian.
508 The Leirdjupet Fault Complex was also active in the Late Permian to Early Triassic, leading to
509 deposition of growth packages in the Bjørnøya Basin described by Blaich et al. (2017) and
510 evident in Figure 2. The age of this faulting is constrained by seismic tie to well 7321/8-1 in the
511 southern Fingerdjupet Subbasin ("Norwegian Petroleum Directorate Factpages," 2017).
512 Reactivation in the Terningen Fault Complex is suggested as a fundamental control on
513 Fingerdjupet Subbasin evolution based on the confident observation of growth packages in Late
514 Permian-Early Triassic strata (Kamp, 2016), in sequences 3 and 5 (Figs. 2, 6, 7, 8), descriptions
515 of Late Triassic growth wedges connected to the Terningen Fault Complex (Kamp, 2016), and
516 evidence for extensional faulting post-dating the youngest preserved basin fill. Based on the
517 current work and observations by Blaich et al. (2017) it is suggested that the Bjørnøya Basin
518 and Fingerdjupet Subbasin shares a common history of reactivation of major, steeply dipping N-

S and NNE-SSW faults from the Late Permian onwards.Orientation of faults may not fully reflect the stress regime at the time of faulting, especially if basement rooted with a strong inherited trend (Sibson, 1985). Depending on changes in the stress regime, reactivation could be favored over establishing new trends, as would be expected for the Terningen Fault Complex and Randi Fault Set. On the other hand, E-W and NW-SE fault sets, which are confined to intervals in the stratigraphy, more likely represent the stress field driving the faulting. It follows from this that significant changes in the local stress regime have occurred several times in basin history, notably (1) between Late Triassic reactivation of the NNE-SSW Terningen Fault Complex (Kamp, 2016) and latest Triassic to Middle Jurassic faulting in the E-W striking fault population; (2) between cessation of extensional faulting in the E-W oriented fault population in the Middle Jurassic and another reactivation of the Terningen Fault Complex in the latest Jurassic to Hauterivian; and (3) during one or several periods in post-Albian times as evident by faulting along NW-SE striking faults and reactivations of NNE-SSW, N-S and E-W striking fault populations. Although further evidence is needed, these inferred changes in the local stress regime are believed to reflect the interplay between North Atlantic and Arctic extensional tectonics as previously suggested by e.g. Faleide et al. (1993b).

6.2 Basin evolution

6.2.1 Latest Triassic to Middle Jurassic extensional faulting

Sequence 1 (intra lower Norian – Oxfordian-Callovian) records an extensional faulting event in the Fingerdjupet Subbasin where growth wedges relate to faults oriented E-W (Fig. 6-Sequence 1). Previous work by Faleide et al. (1993a, 1993b, 2015) and Gabrielsen et al. (1990) have briefly touched upon Jurassic extensional faulting events affecting the Fingerdjupet Subbasin, although limitations in seismic coverage and resolution have made it difficult to decide on the timing of these events and also whether the extensional faulting events were continuous or

545 punctuated by tectonically quiet periods. Faleide et al. (1993a, 1993b) linked a
546 Bathonian/Callovian hiatus in the Hammerfest Basin to the onset of Middle-Late Jurassic
547 tectonics in the Barents Sea and indicated that this tectonic phase likely initiated the subsidence
548 of the Bjørnøya Basin. For the present study, seismic resolution still represents a challenge for
549 deciding on the timing of the extensional faulting event recorded by Sequence 1. This is
550 illustrated by Fig. 4 (inset), where unconformities inferred from biostratigraphic and
551 petrophysical log data are closely spaced in the seismic data. More specific age constraints on
552 this extensional faulting event must be inferred from wells, were the stratigraphic resolution is
553 much higher. One indication for the timing of faulting is an unconformity interpreted from
554 biostratigraphic and petrophysical log data of well 7321/7-1 (Robertson Group, 1989) where
555 Bathonian to middle Bajocian strata are likely to be absent. This hiatus could reflect vertical
556 movements in the area, triggered by faulting, consistent with a late Middle Jurassic rift event.
557 Collanega et al. (2017) suggested E-W faults in the Hoop Fault Complex area were active in the
558 Early Jurassic. Judging from the expansion of strata towards E-W oriented faults in the
559 Fingerdjupet Subbasin; however, faults were likely active also in the latest Triassic (Norian).
560 Higher resolution data will be needed to decide whether the extension was continuous
561 throughout deposition of Sequence 1 or if the observed growth packages result from several
562 phases of extensional faulting. Unconformities within Sequence 1 inferred from well 7321/7-1
563 (Middle Norian-Rhaetian/upper Norian and Bathonian-middle Bajocian inferred absent)
564 (Robertson Group, 1989) suggest the latter. Observations from Edgeøya and Hopen in the
565 northern Barents Sea (Osmundsen et al., 2014) and the Goliat area of the Hammerfest Basin in
566 the southern Barents Sea (Mulrooney et al., 2017) are consistent with observations from the
567 Fingerdjupet Subbasin and indicate the regional significance of extensional faulting in E-W
568 striking faults commencing in the Norian.The interpreted Oxfordian-Callovian surface marks the
569 cessation of activity on E-W striking faults in the Fingerdjupet Subbasin, thus disagreeing with

570 the Late Jurassic faulting inferred by Gabrielsen et al. (1990) and Faleide et al. (1993a) both in
571 terms of fault timing and which fault trends were active.
572 The thickness increase observed locally towards the top of the footwalls of NNE-SSW faults is
573 enigmatic, although seismic interpretation suggests these faults were not active during
574 deposition of sequence 1 (Fig. 6, Sequence 1). Possible explanations include differential
575 compaction where the uplifted footwall was compacted less than the adjacent basin, and/or
576 hydrocarbon-filled sandstones at the crests of rotated fault blocks causing velocity pulldown.
577
578 **6.2.2 Late Jurassic tectonic quiescence**
579 Sequence 2 (Oxfordian-Callovian – Berriasian-Tithonian) is largely undisturbed by the different
580 fault sets present in the Fingerdjupet Subbasin. There is a slight but marked westward thickness
581 increase that can be followed along a smooth, gently curved line for more than 100 km (Fig. 6,
582 Sequence 2). This feature crosses both the NNE-SSW Terningen Fault Complex and many of
583 the E-W oriented faults with no affiliated thickness variations, suggesting the faults were not
584 active upon deposition of Sequence 2. Hence, the westward thinning trend likely has a
585 sedimentary rather than tectonic origin. It is thus considered unlikely that the Late Jurassic
586 tectonism has generated the main (N-S/NNE-SSW) fault trend of the Fingerdjupet Subbasin as
587 previously suggested by Gabrielsen et al. (1990) and Faleide et al. (1993a). This deviates from
588 observations in the Hammerfest Basin, where the Late Jurassic to Early Cretaeous records the
589 culmination of Mesozoic rifting which started in Middle Jurassic times (e.g. Faleide et al.,
590 1993b). Speculatively, a greater part of the SW Barents Sea area, including the Fingerdjupet
591 Subbasin, the western Bjarmeland Platform with the Hoop Fault Complex and Mercurius High
592 (Collanega et al., 2017), and the Hammerfest Basin (Faleide et al., 1993b; Gabrielsen et al.,
593 1990; Indrevær et al., 2016; Mulrooney et al., 2017) experienced Early to Middle Jurassic
594 extensional faulting on E-W faults, while deformation became localized to the Hammerfest Basin
595 as extension persisted through the Late Jurassic to Early Cretaceous. Blaich et al. (2017)

suggested a Late Jurassic extensional event affected the Bjørnøya Basin and Fingerdjupet Subbasin, leading to deposition of Kimmeridgian-Tithonian growth packages along major NE-SW and NNE-SSW faults. Detailed 3D mapping performed for the current work, however, does not support these conclusions; thickness differences in Late Jurassic strata in the Fingerdjupet Subbasin seem unrelated to any fault trends. We therefore conclude that tectonic quiescence prevailed in the Fingerdjupet Subbasin in the Late Jurassic. It can thus be speculated that the influence of North Atlantic tectonics reached the Bjørnøya Basin at this time, but not further east into the Fingerdjupet Subbasin.

6.2.3 Latest Jurassic - Hauterivian extensional faulting

Sequence 3 (Berriasian-Tithonian – intra upper Hauterivian) is clearly affiliated with N-S to NNE-SSW faults, where growth wedges relate to the Terningen Fault Complex and faults in the Randi Fault Set (Fig. 6-Sequence 3, Figs. 7 and 8). Growth wedges that occupy the approximately same stratigraphic position in the Bjørnøya Basin are observed banked onto the Leirdjupet Fault Complex and other large NNE-SSW faults in the basin. This is supported by Blaich et al. (2017), who suggested a Valanginian-Hauterivian extensional phase affected the Bjørnøya Basin, southern Stappen High and Fingerdjupet Subbasin. The Hoop Fault Complex to the east of the study area likely also experienced extension at this time (Fitriyanto, 2011), indicating the semi-regional significance of an extensional faulting event (Figs. 2 and 8).The growth packages related to this faulting have a significantly larger areal extent and time thickness compared to those of the proposed latest Triassic – Middle Jurassic extensional faulting event in the Fingerdjupet Subbasin, thus suggesting both larger sediment supply and that a higher relief bathymetry was generated. Considering there was sedimentation on the uplifted footwall highs in the Randi Fault Set it is suggested that Sequence 3 was deposited in a fully marine environment. This is supported by observations of a Valanginian to Barremian condensed

section with overlying middle Barremian marine clays in a shallow stratigraphic corehole (7320/03-U-01) on the northern Ringsel Ridge (Smelror et al., 1998; Århus et al., 1990). Based on the observations from Sequence 3, a latest Jurassic to Hauterivian extensional faulting event is proposed for the Fingerdjupet Subbasin. This extension by movement on N-S to NNE-SSW faults must represent a change in the local stress regime from the suggested latest Triassic to Middle Jurassic extensional faulting event, when the area experienced activity along E-W oriented faults. The inferred stress-axis change might relate to an increasing influence of rifting in the North Atlantic relative to the Arctic around the Jurassic-Cretaceous transition as previously suggested by Faleide et al. (2008, 1993b). This led to reactivation of major fault complexes such as the Ringvassøy-Loppa Fault Complex, Bjørnøyrenna Fault Complex and Leirdjupet Fault Complex (Blaich et al., 2017; Faleide et al., 1993b).

6.2.4 Hauterivian – Barremian tectonic quiescence and clinoform deposition

Sequence 4 is characterized by the presence of prograding clinoforms on the Bjarmeland Platform, in the Randi Fault Set and in the Fingerdjupet Subbasin (Figs. 7, 8, 11, 12). The dominant SE direction of progradation seen in Fig. 11 on the western edge of the Bjarmeland Platform implies that the system must have travelled past the Randi Fault Set area. With distinct, stepwise thickness increase of the sequence in the Randi Fault Set, the prograding system must have interacted either with active faults or with a fault-controlled topography resulting from earlier events that created an under-filled sink. No apparent growth wedges are observed in Sequence 4 at the bottom of the grabens and half-grabens of the Randi Fault Set. Accordingly, we suggest the prograding system filled relict and underfilled fault bathymetry before advancing further southeast. This contrasts Faleide et al. (1993a, 1993b), who speculated that a Hauterivian/Barremian tectonic event indicated from wells in the Hammerfest Basin should have more strongly affected the Bjørnøya Basin. No clinoform geometries are observed in the Ringsel Ridge, suggesting it was a positive bathymetric feature bounded by

areas of deeper water as the prograding system entered the study area, perhaps as a result of footwall uplift on the Leirdjupet and Terningen fault complexes during the suggested latest Jurassic to Hauterivian extensional faulting event. The SE prograding clinoform system merges with and overlies NW prograding clinoforms on the western Bjarmeland Platform (Fig. 12), thus indicating the presence of an uplifted source area to the south. Different foreset angles might represent differences in parameters related to the paleogeographic setting and grain size distribution (Patruno et al., 2015). The SE prograding system has an inferred source area NW to W of Svalbard, commonly linked to regional uplift on the northern Barents margin related to the HALIP (Faleide et al., 2015, 1993b; Marín et al., 2016; Midtkandal et al., 2015; Midtkandal and Nystuen, 2009; Senger et al., 2014). The long distance to the inferred source area suggests dominantly fine-grained sediments are expected, supported by descriptions of the section in wells 7321/7-1, 7321/8-1 and 7321/9-1 (“Norwegian Petroleum Directorate Factpages,” 2017; Robertson Group, 1989) and consistent with gently dipping clinoforms observed in seismic data in the Fingerdjupet Subbasin and western Bjarmeland Platform. Some caution must be exercised, however; Hinna (2016) observed clinothems pinching out before reaching the well locations (7321/7-1, 7321/8-1 and 7321/9-1). The exploration wells targeted rotated fault blocks along NNE-SSW to N-S faults which were active during the latest Jurassic to Hauterivian extensional faulting event and with associated footwall uplift. The rotated fault blocks may thus have represented bathymetric highs as the clinoform system prograded into the area. Hence, the deposits described in the wells might not fully represent the SE-prograding clinoform system. The steeper foreset angles in the NW prograding system indicate a more proximal position with regards to source area, which together with the Barremian age of the sequence, supports an Early Barremian uplift of the Loppa High as described by Indrevær et al. (2016). Though proximal to the Loppa High, no inversion structures related to this uplift are observed in the study area.

6.2.5 Aptian extensional faulting

Sequence 5 (intra Barremian – intra lower Albian) records a significant extensional faulting event where growth packages are observed along N-S and NNE-SSW oriented faults. They link up with faults active during the proposed Tithonian to Hauterivian extensional faulting event, thus suggesting reactivation as a control on basin development (Fig. 6-Sequence 5). The sequence follows a typical fault system evolution where many faults are involved in the initial nucleation phase but eventually all the extension is focused on a few large faults (Fig. 6-sub-sequence 5A and 5B) (Cowie, 1998). Sub-sequence 5A (intra Barremian – intra Aptian 1) shows growth packages along many faults in the Terningen Fault Complex and the Randi Fault Set, setting up a basin-wide morphology of half-grabens and footwall highs (Fig. 6–sub-sequence 5A, Fig. 7). Sub-sequence 5A is not present on the Ringsel Ridge, possibly as a consequence of footwall uplift in the Terningen and Leirdjupet fault complexes early during the this extensional faulting event, causing subaerial exposure and erosion of Barremian strata. Truncation of strata internally in Sub-sequence 5A in uplifted footwall blocks in the Randi Fault Set suggests some subaerial exposure in the early Aptian, although erosion of these footwall highs was shallower than for the Ringsel Ridge (Fig. 13). The Robertson Group (1989) interpreted marine claystones above and below the intra Aptian 1 surface from cuttings and sidewall cores in well 7321/7-1, suggesting the footwall highs were drowned during continued extensional faulting and deposition of sub-sequence 5B.

The base of sub-sequence 5B marks the end of extensional faulting in the Randi Fault Set as the sub-sequence drapes the footwall highs. A significant thickening towards the Terningen Fault Complex suggests this structure offers the main control on the sediment sink for sub-sequence 5B. The variations in thickness observed across the Terningen Fault Complex decrease up sequence until no difference is observed near the intra Lower Albian horizon, indicating decreasing displacement rates on the controlling faults and/or infill of fault morphology after the end of faulting.

While Sequence 5 contains Barremian to lower Albian strata, an Aptian timing of extensional faulting is suggested on the basis of (1) the deep erosion into Barremian strata in the Ringsel Ridge (Figs. 4, 13); (2) the absence of sub-sequence 5A on the Ringsel Ridge, indicating an early Aptian extensional faulting climax with associated footwall uplift in the Terningen Fault Complex (Figs. 4, 7, 8, 13); and (3) decreasing time thickness differences across the Terningen Fault Complex through the Aptian, with only minor differences for the possible lower Albian strata near the top of sub-sequence 5B (Figs. 4, 7, 8). Faleide et al. (1993a, 1993b) and Blaich et al. (2017) described an Aptian rift event in the Bjørnøya Basin, Fingerdjupet Subbasin and southern Stappen High, where the Ringsel Ridge experienced uplift and erosion. These observations are consistent with the present study, where Barremian strata in the Ringsel Ridge are truncated (Fig. 13) and the unconformity correlates with growth wedges in the Fingerdjupet Subbasin and Bjørnøya Basin (Figs. 2, 7, 8). The extent and thickness of these growth wedges, however, cannot be accounted for by erosion of the Ringsel Ridge alone and indicate additional sediment sources were present.

The Barremian-earliest Aptian magmatism on Svalbard and the shelfal areas to the E and S, seen as flood basalts and intrusive dykes and sills and described by e.g. Grogan et al. (2000), Maher (2001), Minakov et al. (2012) and Polteau et al. (2016), follows a NNE grain. The magmatism on Svalbard and Franz Josef Land is suggested to result from a distinct magmatic event at 125 Ma (Polteau et al., 2016), essentially contemporaneously with extensional faulting in the Terningen Fault Complex, Randi Fault Set and Leirdjupet Fault Complex. This indicates a link to the Fingerdjupet Subbasin and Bjørnøya Basin where Aptian extension is evident as normal faulting with associated sedimentary growth packages in the Terningen Fault Complex, Leirdjupet Fault Complex and other faults. The extension across the entire western Barents shelf likely relates to the northward propagation of Atlantic rifting (Blaich et al., 2017; Faleide et al., 2008, 1993b) while the manifestation of the extension, speculatively, might vary as a function of proximity to the HALIP. Atlantic influence on areas adjacent to the Fingerdjupet

Subbasin is evident from documented extensional faulting in the Polhem Subplatform and the Ringvassøy-Loppa and Bjørnøyrenna fault complexes (Indrevær et al., 2016).

6.2.6 Albian tectonic quiescence and post-late Albian extensional faulting

Sequence 6 (intra lower Albian - URU) represents a conformable succession of Albian strata in the Fingerdjupet Subbasin. The Fingerdjupet Subbasin was still a sediment sink in the early Albian as indicated by onlaps onto the slope towards the Bjarmeland Platform, which was subsequently draped by upper Albian strata. Sequence 6 is offset by faults with orientations NNE-SSW, E-W and NW-SE (Figs. 10, 7, and 8). The timing of the tectonic events related to these faults, however, is difficult to constrain in the Fingerdjupet Subbasin both because of the lack of growth wedges related to the faults and also because the faults are commonly truncated at the URU. The post-Early Cretaceous development of the basin must be examined indirectly by studying neighboring basins where post-Lower Cretaceous deposits have been preserved. This is beyond scope for the present work. The orientations of the fault systems affecting Sequence 6 indicate not only reactivation of faults related to the proposed latest Triassic-Middle Jurassic and Barremian-lower Albian extensional faulting events, but likely also a change in the direction of extension leading to faulting along NW-SE oriented faults. The limited preserved stratigraphy and lack of confident observations of cross-cutting relationships makes it difficult to establish a sequence of events for the younger fault activity. It likely reflects varying stress regimes and fault styles during the Late Cretaceous and Paleogene extension leading to breakup and seafloor spreading in the Norwegian-Greenland Sea in the Eocene (Faleide et al., 2008).

7. Conclusions

- The Fingerdjupet Subbasin has an evolution closely linked to reactivation of a N-S to NNE-SSW extensional fabric established in the Late Permian possibly following thrusting and extensional collapse in the Caledonian Orogen in the Silurian and Devonian and an inferred Carboniferous extensional reactivation. The Bjørnøya Basin and Fingerdjupet Subbasin share a common history of extensional faulting and reactivation on steeply dipping N-S to NNE-SSW faults from the Late Permian onwards. The Fingerdjupet Subbasin evolved as a semi-regional rollover structure where the Bjarmeland Platform was repeatedly downfaulted in the Terningen Fault Complex, creating accommodation space in the hangingwall. The Randi Fault Set developed as a result of outer-arc extension and breakdown faulting in the crest of the rollover anticline.

- Extension led to normal faulting on E-W striking faults from the latest Triassic to late Middle Jurassic in the Fingerdjupet Subbasin and adjacent areas. This extensional faulting event likely affected a very large area, suggested by recent observations from other workers north (Edgeøya and Hopen) and south (Hammerfest Basin) in the western Barents Sea.

- Late Jurassic tectonic quiescence in the study area contrast Late Jurassic to earliest Cretaceous extensional faulting on E-W striking faults in the Hammerfest Basin.

- Reactivation in the Terningen Fault Complex, Randi Fault Set and other N-S and NNE-SSW faults in the latest Jurassic to Hauterivian established the Fingerdjupet Subbasin as a major Lower Cretaceous depocenter. The study area remained submerged through this phase of extensional faulting and the relief generated by faulting was not filled. The change in the local stress regime leading up to this extensional faulting likely relates to an increasing influence of rifting in the North Atlantic relative to the Arctic.

- During Barremian tectonic quiescence, SE prograding deltaic deposits derived from an uplifted region NW of Svalbard filled the Fingerdjupet Subbasin before prograding further SE on the Bjarmeland Platform. Early Barremian uplift of the Loppa High resulted in NW prograding clinoforms on the western Bjarmeland Platform.

- Reactivation of major fault complexes in the SW Barents Sea, including the Terningen and Leirdjupet fault complexes, occurred in the Aptian, leading to subaerial exposure of the Ringsel Ridge and footwall highs in the Randi Fault Set. Sedimentary growth wedges received sediments from these proximal sources as well as distal sources.

- Post-upper Albian extension led to both reactivation of E-W and N-S to NNE-SSW extensional fabrics and faulting along NW-SE striking faults, reflecting a changing stress regime during Late Cretaceous-Paleogene extension and subsequent breakup and seafloor spreading in the North Atlantic.

8. Acknowledgements

We thank the LoCrA consortium (Lower Cretaceous basin studies in the Arctic) for financial support, TGS for allowing us to publish seismic data and Schlumberger for providing us with academic software licenses for Petrel 2015. Alf Eivind Ryseth and one anonymous reviewer are thanked for thorough reviews and insightful comments which helped improve the quality of the manuscript.

9. Reference list

Baig, I., Faleide, J.I., Jahren, J., Mondol, N.H., 2016. Cenozoic exhumation on the southwestern Barents Shelf: Estimates and uncertainties constrained from compaction and thermal maturity analyses. Mar. Pet. Geol. 73, 105–130. doi:10.1016/j.marpetgeo.2016.02.024

Barrère, C., Ebbing, J., Gernigon, L., 2009. Offshore prolongation of Caledonian structures and basement characterisation in the western Barents Sea from geophysical modelling. Tectonophysics 470, 71–88. doi:10.1016/j.tecto.2008.07.012

Blaich, O.A., Tsikalas, F., Faleide, J.I., 2017. New insights into the tectono-stratigraphic evolution of the southern Stappen High and its transition to Bjørnøya Basin, SW Barents Sea. Mar. Pet. Geol. 85, 89–105. doi:10.1016/j.marpetgeo.2017.04.015

Breivik, A.J., Faleide, J.I., Gudlaugsson, S.T., 1998. Southwestern Barents Sea margin: late Mesozoic sedimentary basins and crustal extension. Tectonophysics 293, 21–44. doi:10.1016/S0040-1951(98)00073-0

Breivik, A.J., Mjelde, R., Grogan, P., Shimamura, H., Murai, Y., Nishimura, Y., 2003. Crustal structure and transform margin development south of Svalbard based on ocean bottom seismometer data. Tectonophysics 369, 37–70. doi:10.1016/S0040-1951(03)00131-8

Braathen, A., Bergh, S.G., Maher, H.D., 1999a. Application of a critical wedge taper model to the tertiary transpressional fold-thrust belt on Spitsbergen, Svalbard. Bull. Geol. Soc. Am. 111, 1468–1485. doi:10.1130/0016-7606(1999)111<1468:AOACWT>2.3.CO;2

Braathen, A., Maher, H.D., Haabet, T.E., Kristensen, S.E., Tørudbakken, B.O., Worsley, D., 1999b. Caledonian thrusting on Bjornoya: Implications for Palaeozoic and Mesozoic tectonism of the western Barents Shelf. Nor. Geol. Tidsskr. 79, 57–68. doi:10.1080/002919699433915

Collanega, L., Massironi, M., Breda, A., Kjølhamar, B.E., 2017. Onset of N-Atlantic rifting in the Hoop Fault Complex (SW Barents Sea): An orthorhombic dominated faulting?

Tectonophysics 706–707, 59–70. doi:10.1016/j.tecto.2017.04.003

Corfu, F., Polteau, S., Planke, S., Faleide, J.I., Svensen, H., Zayoncheck, A., Stolbov, N., 2013. U-Pb geochronology of Cretaceous magmatism on Svalbard and Franz Josef Land, Barents Sea large igneous province. Geol. Mag. 150, 1127–1135. doi:http://dx.doi.org/10.1017/S0016756813000162

Cowie, P.A., 1998. A healing-reloading feedback control on the growth rate of seismogenic faults. J. Struct. Geol. 20, 1075–1087. doi:10.1016/S0191-8141(98)00034-0

Dengo, C.A., Røssland, K.G., 1992. Extensional tectonic history of the western Barents Sea, in: Larsen, R.M., Brekke, H., Larsen, B.T., Talleraas, E. (Eds.), Structural and Tectonic Modelling and Its Application to Petroleum Geology, NPF Special Publication 1. Elsevier, pp. 91–107.

Dimakis, P., Braathen, B.I., Faleide, J.I., Elverhøi, A., Gudlaugsson, S.T., 1998. Cenozoic erosion and the preglacial uplift of the Svalbard-Barents Sea region. Tectonophysics 300, 311–327. doi:10.1016/S0040-1951(98)00245-5

Doré, A.G., 1991. Structural foundation and evolution of Mesozoic Seaways between Europe and the Arctic. Palaeogeogr. Palaeoclimatol. Palaeoecol. 87, 441–492.

Faleide, J.I., Bjørlykke, K., Gabrielsen, R.H., 2015. Geology of the Norwegian Continental Shelf, in: Bjørlykke, K. (Ed.), Petroleum Geoscience: From Sedimentary Environments to Rock Physics, Second Edition. Springer-Verlag, pp. 603–637. doi:10.1007/978-3-642-34132-8

Faleide, J.I., Solheim, A., Fiedler, A., Hjelstuen, B.O., Andersen, E.S., Vanneste, K., 1996. Late Cenozoic evolution of the western Barents Sea-Svalbard continental margin. Glob. Planet. Change 12, 53–74. doi:10.1016/0921-8181(95)00012-7

Faleide, J.I., Tsikalas, F., Mjelde, R., Wilson, J., Eldholm, O., 2008. Structure and evolution of the continental margin off Norway and the Barents Sea. Episodes 31, 82–91.

Faleide, J.I., Vågnes, E., Gudlaugsson, S.T., 1993a. Late Mesozoic-Cenozoic evolution of the southwestern Barents Sea. Geol. Soc. London, Pet. Geol. Conf. Ser. 4, 933–950.

843 Faleide, J.I., Vågnes, E., Gudlaugsson, S.T., 1993b. Late Mesozoic-Cenozoic evolution of the
844 south-western Barents Sea in a regional rift-shear tectonic setting. Mar. Pet. Geol.
845 doi:10.1016/0264-8172(93)90104-Z
846 Fitriyanto, A., 2011. Structural Analysis of The Hoop Fault Complex, SW Barents Sea. MSc
847 Thesis, University of Oslo.
848 Friedmann, S.J., Burbank, D.W., 1995. Rift basins and supradetachment basin: intracontinental
849 extensional end members. Basin Res. 7, 109–127.
850 Gabrielsen, R.H., Faerseth, R.B., Jensen, L.N., Kalheim, J.E., Riis, F., 1990. Structural
851 Elements of the Norwegian continental shelf. Part 1: The Barents Sea Region. NPD- Bull.
852 No.6, 33 pp.
853 Gabrielsen, R.H., Grunnaleite, I., Rasmussen, E., 1997. Cretaceous and tertiary inversion in the
854 Bjørnøyrenna Fault Complex, south-western Barents Sea. Mar. Pet. Geol.
855 doi:10.1016/S0264-8172(96)00064-5
856 Gernigon, L., Brönner, M., 2012. Late Palaeozoic architecture and evolution of the southwestern
857 Barents Sea : insights from a new generation of aeromagnetic data. J. Geol. Soc. London
858 169, 1–11. doi:10.1144/0016-76492011-131
859 Gernigon, L., Brönner, M., Roberts, D., Olesen, O., Nasuti, A., Yamasaki, T., 2014. Crustal and
860 basin evolution of the southwestern Barents Sea: From Caledonian orogeny to continental
861 breakup. Tectonics 33, 347–373. doi:10.1002/2013TC003439
862 Glørstad-Clark, E., 2011. Basin analysis in the western Barents Sea area: The interplay
863 between accomodation space and depositional systems. PhD Thesis University of Oslo.
864 Glørstad-Clark, E., Faleide, J.I., Lundschien, B.A., Nystuen, J.P., 2010. Triassic seismic
865 sequence stratigraphy and paleogeography of the western Barents Sea area. Mar. Pet.
866 Geol. 27, 1448–1475. doi:10.1016/j.marpetgeo.2010.02.008
867 Gradstein, F.M., Ogg, J.G., Hilgen, F.J., 2012. On The Geologic Time Scale. Newsletters
868 Stratigr. 45, 171–188. doi:10.1127/0078-0421/2012/0020

Grogan, P., Nyberg, K., Fotland, B., Myklebust, R., Dahlgren, S., Riis, F., 2000. Cretaceous magmatism south and east of Svalbard: Evidence from seismic reflection and magnetic data. Polarforschung 68, 25–34.

Gudlaugsson, S.T., Faleide, J.I., 1994. The continental margin between Spitsbergen and Bjørnøya, Seismic Atlas of Western Svalbard: A selection of regional seismic transects 130. Norwegian Polar Institute.

Gudlaugsson, S.T., Faleide, J.I., Johansen, S.E., Breivik, a. J., 1998. Late Palaeozoic structural development of the South-western Barents Sea. Mar. Pet. Geol. 15, 73–102. doi:10.1016/S0264-8172(97)00048-2

Henriksen, E., Bjornseth, H.M., Hals, T.K., Heide, T., Kiryukhina, T., Klovjan, O.S., Larssen, G.B., Ryseth, A.E., Ronning, K., Sollid, K., Stoupakova, A., 2011a. Uplift and erosion of the greater Barents Sea: impact on prospectivity and petroleum systems. Geol. Soc. London, Mem. 35, 271–281. doi:10.1144/M35.17

Henriksen, E., Ryseth, A.E., Larssen, G.B., Heide, T., Ronning, K., Sollid, K., Stoupakova, a. V., 2011b. Chapter 10 Tectonostratigraphy of the greater Barents Sea: implications for petroleum systems. Geol. Soc. London, Mem. 35, 163–195. doi:10.1144/M35.10

Hinna, C.H., 2016. Seismic Characterization of Lower Cretaceous Clinoform Packages in the Fingerdjupet Sub-basin, Southwestern Barents Sea. MSc Thesis, University of Stavanger.

Hongbin Xiao, Suppe, J., 1992. Origin of rollover. Am. Assoc. Pet. Geol. Bull. doi:10.1306/BDFF8CD6-1718-11D7-8645000102C1865D

Indrevær, K., Bergh, S.G., Koehl, J.B., Hansen, J.A., Schermer, E.R., Ingebrigtsen, A., 2013. Post-Caledonian brittle fault zones on the hyperextended SW Barents Sea margin: New insights into onshore and offshore margin architecture. Nor. Geol. Tidsskr. 93, 167–188.

Indrevær, K., Gabrielsen, R.H., Faleide, J.I., 2016. Early Cretaceous synrift uplift and tectonic inversion in the Loppa High area, southwestern Barents Sea, Norwegian shelf. J. Geol. Soc. London. jgs2016-066. doi:10.1144/jgs2016-066

895 Jakobsson, M., Mayer, L., Coakley, B., Dowdeswell, J.A., Forbes, S., Fridman, B., Hodnesdal,
896 H., Noormets, R., Pedersen, R., Rebesco, M., Schenke, H.W., Zarayskaya, Y., Accettella,
897 D., Armstrong, A., Anderson, R.M., Bienhoff, P., Camerlenghi, A., Church, I., Edwards, M.,
898 Gardner, J. V., Hall, J.K., Hell, B., Hestvik, O., Kristoffersen, Y., Marcussen, C.,
899 Mohammad, R., Mosher, D., Nghiem, S. V., Pedrosa, M.T., Travaglini, P.G., Weatherall,
900 P., 2012. The International Bathymetric Chart of the Arctic Ocean (IBCAO) Version 3.0.
901 Geophys. Res. Lett. 39, 1–6. doi:10.1029/2012GL052219
902 Kamp, W.K., 2016. Permian to Late Triassic structural and stratigraphic evolution of the
903 Fingerdjupet Subbasin. MSc Thesis, University of Oslo.
904 Laberg, J.S., Andreassen, K., Vorren, T.O., 2012. Late cenozoic erosion of the high-latitude
905 southwestern barents sea shelf revisited. Bull. Geol. Soc. Am. 124, 77–88.
906 doi:10.1130/B30340.1
907 Larssen, G.B., Elvebakk, G., Henriksen, L.B., Nilsson, I., Samuelsberg, T.J., Stemmerik, L.,
908 Worsley, D., Kristensen, S.E., Svånå, T.A., 2002. Upper Palaeozoic lithostratigraphy of the
909 Southern Norwegian Barents Sea. Nor. Pet. Dir. Bull. 9, 76.
910 Maher, H.D., 2001. Manifestations of the Cretaceous High Arctic Large Igneous Province in
911 Svalbard. J. Geol. 109, 91–104. doi:10.1130/2007.2431
912 Marín, D., Escalona, A., Śliwińska, K.K., Nøhr-Hansen, H., Mordasova, A., 2016. Sequence
913 stratigraphy and lateral variability of Lower Cretaceous clinoforms in the southwestern
914 Barents Sea. Am. Assoc. Pet. Geol. Bull. 20, 221. doi:10.1306/10241616010
915 Mauduit, T., Brun, J.P., 1998. Growth fault / rollover systems: Birth, growth and decay. J.
916 Geophys. Res. 103, 18 119-18 136.
917 McClay, K.R., 1990. Extensional fault systems in sedimentary basins: a review of analogue
918 model studies. Mar. Pet. Geol. 7, 206–233. doi:10.1016/0264-8172(90)90001-W
919 Midtkandal, I., Faleide, J.I., Planke, S., Myrsini, D., Dahlberg, M., Myklebust, R., Nystuen, J.P.,
920 Torsvik, T.H., 2015. Source-to-sink Dynamics in the Early Cretaceous Boreal Basin;

921 Progradational Lobes from a Missing Source. Am. Geophys. Union, Fall Meet. 2015, Abstr.
922 #T51B-2876.
923 Midtkandal, I., Nystuen, J.P., 2009. Depositional architecture of a low-gradient ramp shelf in an
924 epicontinental sea: The lower Cretaceous of Svalbard. Basin Res. 21, 655–675.
925 doi:10.1111/j.1365-2117.2009.00399.x
926 Minakov, A., Mjelde, R., Faleide, J.I., Flueh, E.R., Dannowski, A., Keers, H., 2012. Mafic
927 intrusions east of Svalbard imaged by active-source seismic tomography. Tectonophysics
928 518–521, 106–118. doi:10.1016/j.tecto.2011.11.015
929 Mulrooney, M.J., Leutscher, J., Braathen, A., 2017. A 3D structural analysis of the Goliat field,
930 Barents Sea, Norway. Mar. Pet. Geol. 86, 192–212. doi:10.1016/j.marpetgeo.2017.05.038
931 Norwegian Petroleum Directorate Factpages [WWW Document], 2017. URL
932 http://factpages.npd.no (accessed 3.2.17).
933 Osmundsen, P.T., Braathen, A., Rød, R.S., Hynne, I.B., 2014. Styles of normal faulting and
934 fault-controlled sedimentation in the Triassic deposits of Eastern Svalbard. Nor. Pet. Dir.
935 Bull. 11, 61–79.
936 Patruno, S., Hampson, G.J., Jackson, C.A.L., Dreyer, T., 2015. Clinoform geometry,
937 geomorphology, facies character and stratigraphic architecture of a sand-rich subaqueous
938 delta: Jurassic Sognefjord Formation, offshore Norway. Sedimentology 62, 350–388.
939 doi:10.1111/sed.12153
940 Peron-Pinvidic, G., Manatschal, G., Minshull, T.A., Sawyer, D.S., 2007. Tectonosedimentary
941 evolution of the deep Iberia-Newfoundland margins: Evidence for a complex breakup
942 history. Tectonics 26, 1–19. doi:10.1029/2006TC001970
943 Polteau, S., Hendriks, B.W.H., Planke, S., Ganerød, M., Corfu, F., Faleide, J.I., Midtkandal, I.,
944 Svensen, H.S., Myklebust, R., 2016. The Early Cretaceous Barents Sea Sill Complex:
945 Distribution, 40Ar/39Ar geochronology, and implications for carbon gas formation.
946 Palaeogeogr. Palaeoclimatol. Palaeoecol. 441, 83–95. doi:10.1016/j.palaeo.2015.07.007

947 Ritzmann, O., Faleide, J.I., 2007. Caledonian basement of the western Barents Sea. Tectonics
948 26, 1–20. doi:10.1029/2006TC002059
949 Robertson Group, 1989. Mobil 7321/7-1 Norwegian Barents Sea well: Biostratigraphy of the
950 interval 613m(SWC)-3552mTD.
951 Rønnevik, H., Jacobsen, H.-P., 1984. Petroleum Geology of the North European Margin:
952 Proceedings of the North European Margin Symposium (NEMS ’83), organized by the
953 Norwegian Petroleum Society and held at the Norwegian Institute of Technology (NTH) in
954 Trondheim 9--11 May, 1983, in: Spencer, A.M. (Ed.), . Springer Netherlands, Dordrecht,
955 pp. 19–32. doi:10.1007/978-94-009-5626-1_3
956 Senger, K., Tveranger, J., Ogata, K., Braathen, A., Planke, S., 2014. Late Mesozoic magmatism
957 in Svalbard: A review. Earth-Science Rev. 139, 123–144.
958 doi:10.1016/j.earscirev.2014.09.002
959 Sibson, R.H., 1985. A note on fault reactivation. J. Struct. Geol. 7, 751–754. doi:10.1016/0191-
960 8141(85)90150-6
961 Smelror, M., Mørk, A., Monteil, E., Rutledge, D., Leereveld, H., 1998. The Klippfisk formation - a
962 new lithostratigraphic unit of Lower Cretaceous platform carbonates on the Western
963 Barents Shelf. Polar Res. doi:10.1111/j.1751-8369.1998.tb00271.x
964 Solheim, A., Kristoffersen, Y., 1984. Sediments above the upper regional unconformity:
965 thickness, seismic stratigraphy and outline of the glacial history. Nor. Polarinst. 179, 1–26.
966 Svennevig, K., Guarnieri, P., Stemmerik, L., 2017. 3D restoration of a Cretaceous rift basin in
967 Kilen, eastern North Greenland. Nor. J. Geol. 97, 21–32. doi:10.17850/njg97-1-02
968 Vågnes, E., Gabrielsen, R.H., Haremo, P., 1998. Late Cretaceous-Cenozoic intraplate
969 contractional deformation at the Norwegian continental shelf: Timing, magnitude and
970 regional implications. Tectonophysics 300, 29–46. doi:10.1016/S0040-1951(98)00232-7
971 Worsley, D., Agdestein, T., Gjelberg, J.G., Kirkemo, K., Mørk, A., Nilsson, I., Olaussen, S.,
972 Steel, R.J., Stemmerik, L., 2001. The geological evolution of Bjørnøya, Arctic Norway:

Implications for the Barents Shelf. Nor. Geol. Tidsskr. 81, 195–234.

Århus, N., A Kelly, S.R., H Collins, J.S., Sandy, M.R., Grooe, O., Dulwich London, E.S., 1990. Systematic palaeontology and biostratigraphy of two Early Cretaceous condensed sections from the Barents Sea. Polar Res. 8, 165–194.

10. Figure captions

Fig. 1: Map showing study area in the southwestern Barents Sea with structural elements, exploration wells, shallow coreholes and location of presented seismic profiles. a) Arctic overview map, SW Barents Sea indicated in red box. Abbreviations: HFZ: Hornsund Fault Zone, SFZ: Senja Fracture Zone. Modified from Jakobsson et al. (2012). b) SW Barents Sea basins and highs. Green outline indicate 3D seismic cube used for this study, stippled red line indicates location of Fig. 2 and red box indicate study area. Basin colours indicate main periods of basin formation according to Faleide et al. (2015): Red corresponds to Late Paleozoic, blue corresponds to Late Jurassic – Early Cretaceous and yellow corresponds to Late Cretaceous – Paleocene. Abbreviations: BB: Bjørnøya Basin, BjFC: Bjørnøyrenna Fault Complex, FSB: Fingerdjupet Subbasin, HfB: Hammerfest Basin, HFC: Hoop Fault Complex, HFZ: Hornsund Fault Zone, LH: Loppa High, MB: Maud Basin, MH: Mercurius High, NB: Nordkapp Basin, NH: Norsel High, OB: Ottar Basin, PSP: Polhem Subplatform, RLFC: Ringvassøy-Loppa Fault Complex, SFZ: Senja Fracture Zone, SR: Senja Ridge, SH: Stappen High, SB: Sørvestsnaget Basin, TFFC: Troms-Finnmark Fault Complex, TB: Tromsø Basin, VH: Veslemøy High, VVP: Vestbakken Volcanic Province. Map modified from (Faleide et al., 2015). c) Berriasian-Tithonian time structure map showing the main structural elements in the study area. Three structural elements have been defined in this work: The Ringsel Ridge, Terningen Fault Complex and Randi Fault Set. Some important faults are indicated in dark grey. Green outline indicates extent of 3D seismic data used for this study. Black stippled lines define locations of shown seismic sections. Seismic data courtesy of TGS.

Fig. 2: Composite seismic profile showing the main structural elements of the study area and adjacent region. Major structures are; from E to W; Hoop Fault Complex, Bjarmeland Platform, Randi Fault Set (Appendix), Fingerdjupet Subbasin, Terningen Fault Complex (Appendix),

Ringsel Ridge (Appendix), Leirdjupet Fault Complex and Bjørnøya Basin. Dotted lines indicate changes in seismic line direction and boundaries between different seismic datasets. Profile location is given in Fig. 1b. Seismic data courtesy of TGS.

Fig. 3: Correlation of lithostratigraphic groups from wells 7321/7-1, 7321/8-1 and 7321/9-1 in the Fingerdjupet Subbasin. Stippled outline indicates stratigraphy in focus for the present work. Gamma ray logs and well information from "Norwegian Petroleum Directorate Factpages" (2017).

Fig. 4: Composite seismic profile showing seismic tie to exploration well 7321/7-1. Seismic packages that are barely within seismic resolution on the highs relate to expanded packages in the basin. Inset shows lowermost Cretaceous, Jurassic and uppermost Triassic succession where four unconformities within 150 m (annotated yellow) are interpreted from biostratigraphic and petrophysical log data (Robertson Group plc, 1989). Seismic line bend indicated by black vertical line. Location of seismic line is shown in Fig. 1c. Abbreviations: ilN: intra lower Norian, OC: Oxfordian-Callovian, BT: Berriasian-Tithonian, iuH: intra upper Hauterivian, iB: intra Barremian, ilA: intra lower Aptian, iA1: intra Aptian 1, iA2: intra Aptian 2, ilAl: intra lower Albian, lmA: lower-middle Albian. Seismic data courtesy of TGS.

Fig. 5: Seismic stratigraphic framework of the Late Triassic to Albian succession of the Fingerdjupet Subbasin. The Jurassic and Cretaceous basin evolution is the main focus of the present work and for the Norian to Middle Jurassic (~218-168 Ma), which in the study area corresponds to a relatively thin sedimentary package, is therefore hidden in the chronostratigraphy column. Chronostratigraphic chart modified from Gradstein et al. (2012).

Fig. 6: Time thickness maps and seismic sections for sequences 1, 2, 3, 4, 5A and 5B. Wedge-shaped seismic packages consistent with syn-tectonic deposition are seen for sequences 1 (Intra lower Norian – Oxfordian-Callovian), 3 (Berriasian-Tithonian – intra upper Hauterivian)

and 5 (Intra Barremian – intra lower Albian). Red arrows indicate thickness variations for the sequences. Seismic profile locations are indicated in the respective time thickness maps. Seismic data courtesy of TGS.

Fig. 7: Seismic profile showing the Triassic to Lower Cretaceous succession of the Fingerdjupet Subbasin. Colour overlays correspond to interpreted sequences as outlined in Fig. 5. Wedge-shaped seismic packages and pronounced thickness differences between the Fingerdjupet Subbasin and the Ringsel Ridge are seen for sequences 3 (BT – iuH) and 5 (iB – ilA). The strong, cross-cutting reflections seen in the upper part of the section, particularly near the Ringsel Ridge, are NW-SE oriented faults cut along strike by the seismic profile. Profile location is given in Fig. 1c. Seismic data courtesy of TGS.

Fig. 8: Seismic profile showing the northern Bjørnøya Basin and the Fingerdjupet Subbasin separated by the Ringsel Ridge. The Leirdjupet Fault Complex marks the western boundary of the Ringsel Ridge while the Terningen Fault Complex marks the eastern boundary. Colour overlays correspond to interpreted seismic sequences (Fig. 5). Sequences 3 (BT – iuH) and 5 (iB – ilA) show wedge-shaped seismic geometries in the Fingerdjupet Subbasin and the Bjørnøya Basin and pronounced thickness differences compared to the Ringsel Ridge. Profile location is seen in Fig. 1c. Seismic data courtesy of TGS.

Fig. 9: Seismic section showing transverse folds related to fault displacement gradients and relay zones in the Terningen Fault Complex. Profile is taken along strike and close to a large fault in the hangingwall of the Terningen Fault Complex. Location of seismic line is shown in Fig. 1c. Seismic data courtesy of TGS.

Fig. 10: Variance attribute draped on lower-middle Albian horizon (10a) and upper Albian horizon (10b) highlighting fault trends affecting the Albian succession. Dominant fault

populations are oriented NW-SE and NNE-SSW with a minor influence from E-W oriented faults. Seismic data courtesy of TGS.

Fig. 11: Seismic profile showing prograding clinoforms of Sequence 4 (Fig. 5) in the Randi Fault Set and on the Bjarmeland Platform. The clinoforms show a SE direction of progradation. Location of profile is shown in Fig. 1c. Seismic data courtesy of TGS.

Fig. 12: Seismic profile showing two separate systems of prograding clinoforms in Sequence 4 (Fig. 5) on the Bjarmeland Platform. The low-angled, southeast prograding clinoforms correspond to the system seen in Fig. 11. The seismic line azimuth represents depositional dip for both systems. Location of profile is seen in Fig. 1c. Seismic data courtesy of TGS.

Fig. 13: Seismic sections showing truncation of seismic reflections in the Ringsel Ridge (a, b) and uplifted footwall highs in the Fingerdjupet Subbasin (c). Locations of seismic profiles are given in Fig. 1c. Seismic data courtesy of TGS.

11. Figures

Fig.1:

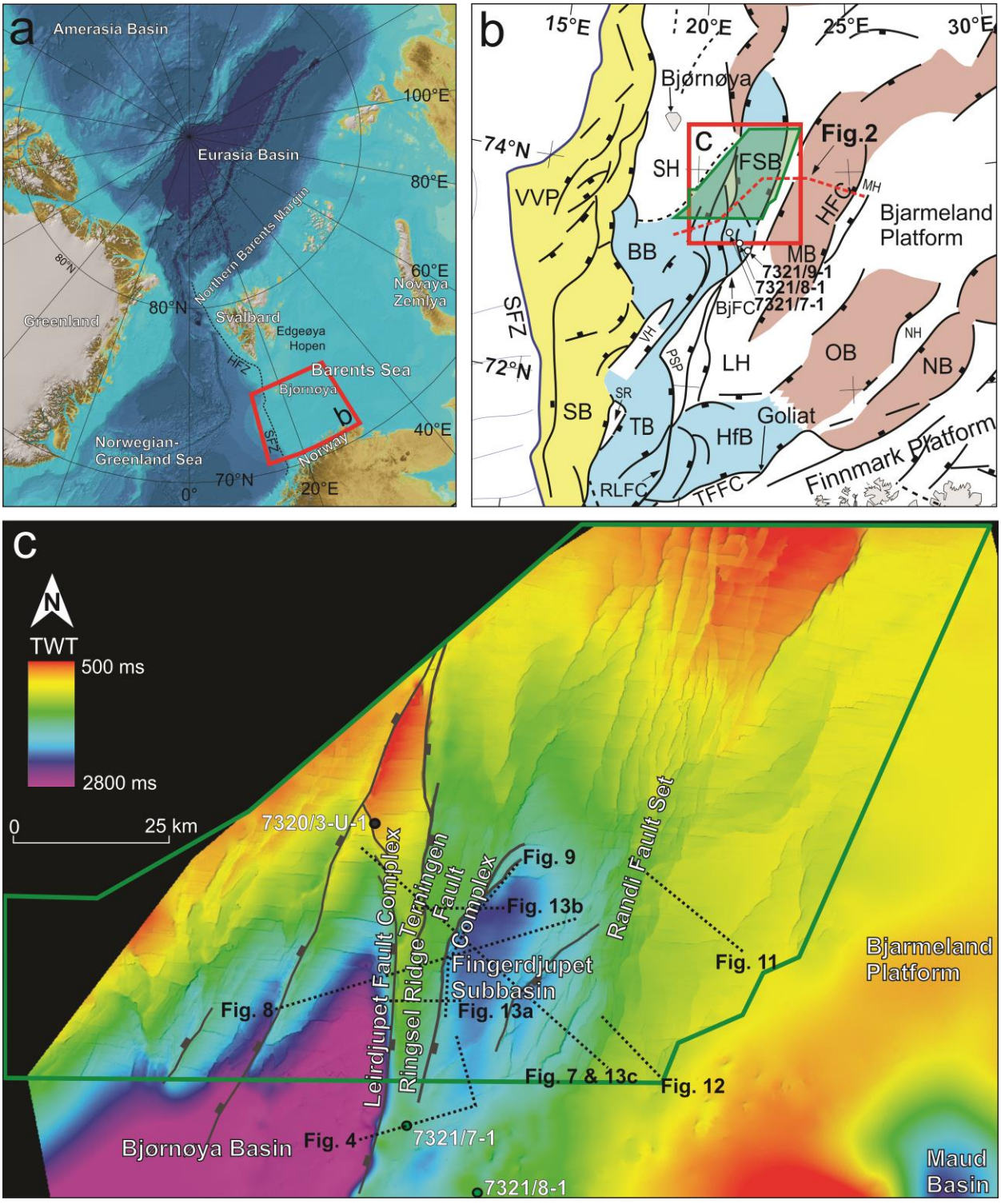

1068 *Fig. 2:*

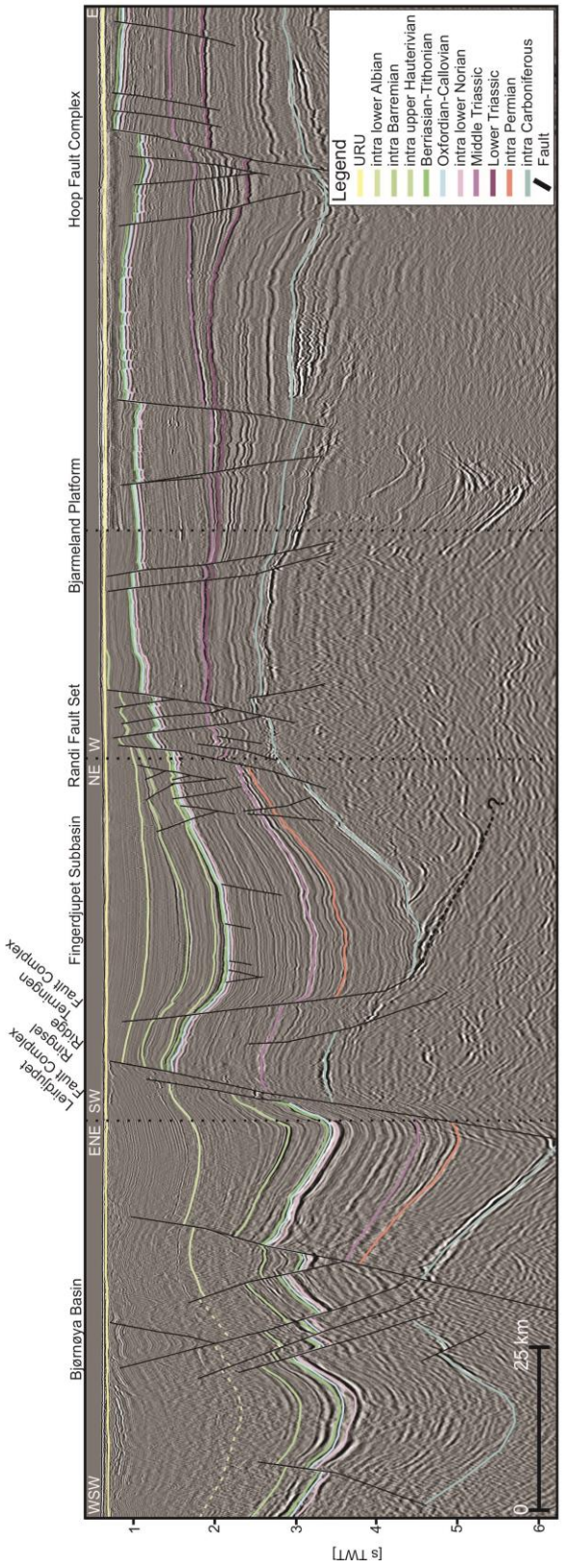

1069

1070 *Fig. 3:*

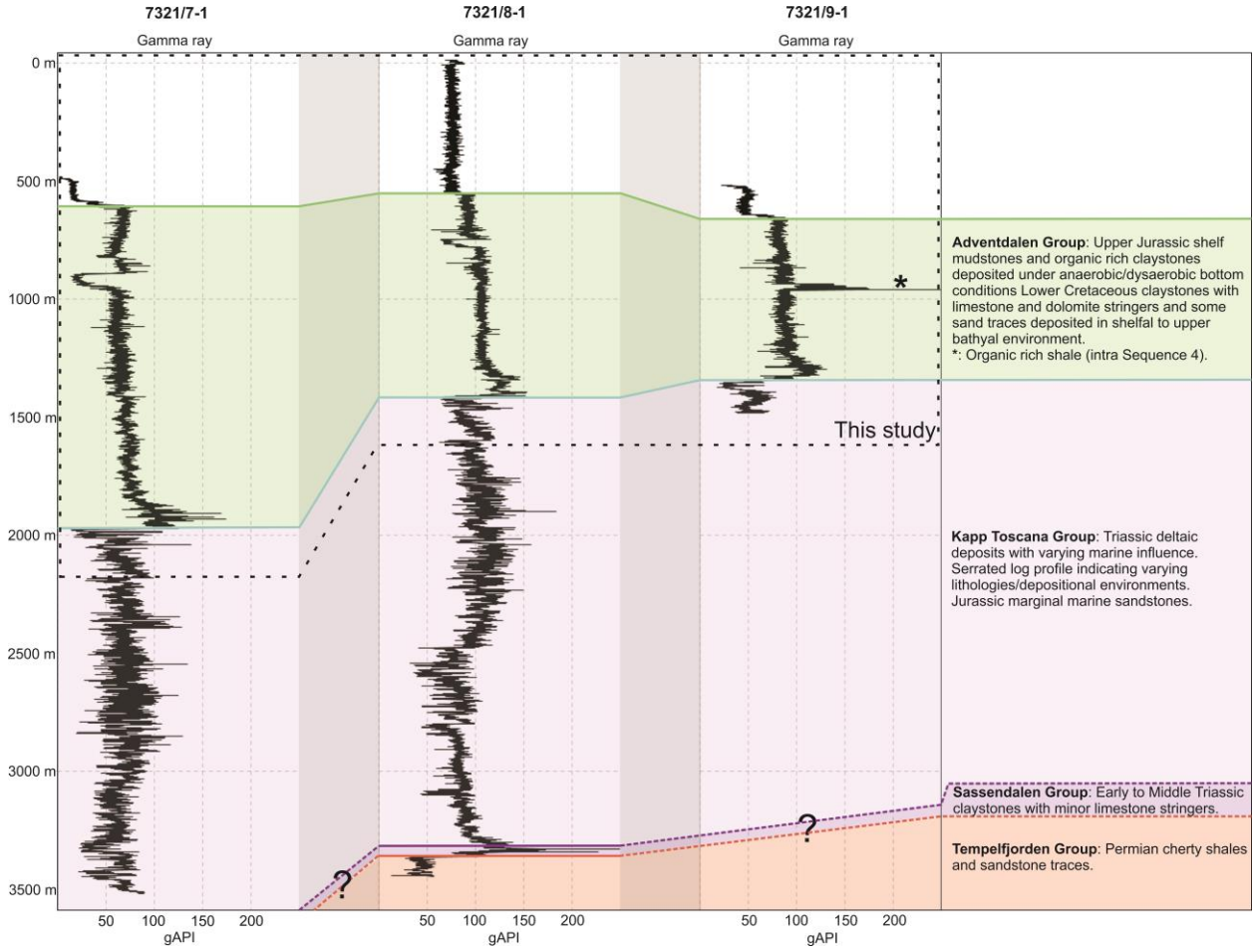

1071

1072 *Fig. 4:*

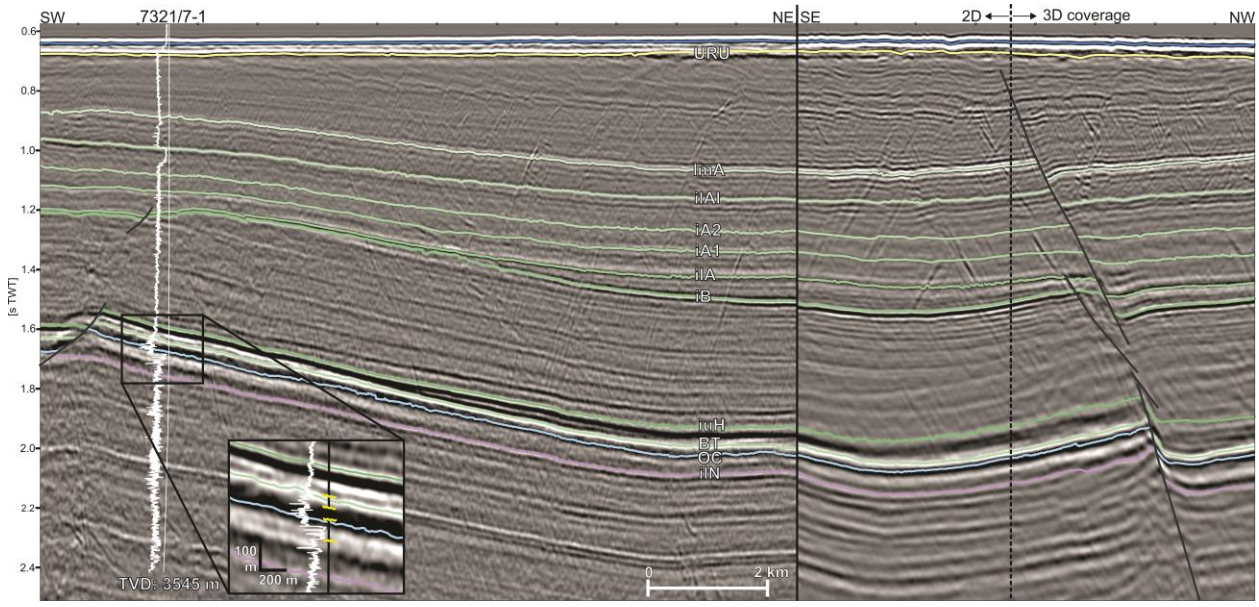

1073

1074 *Fig. 5:*

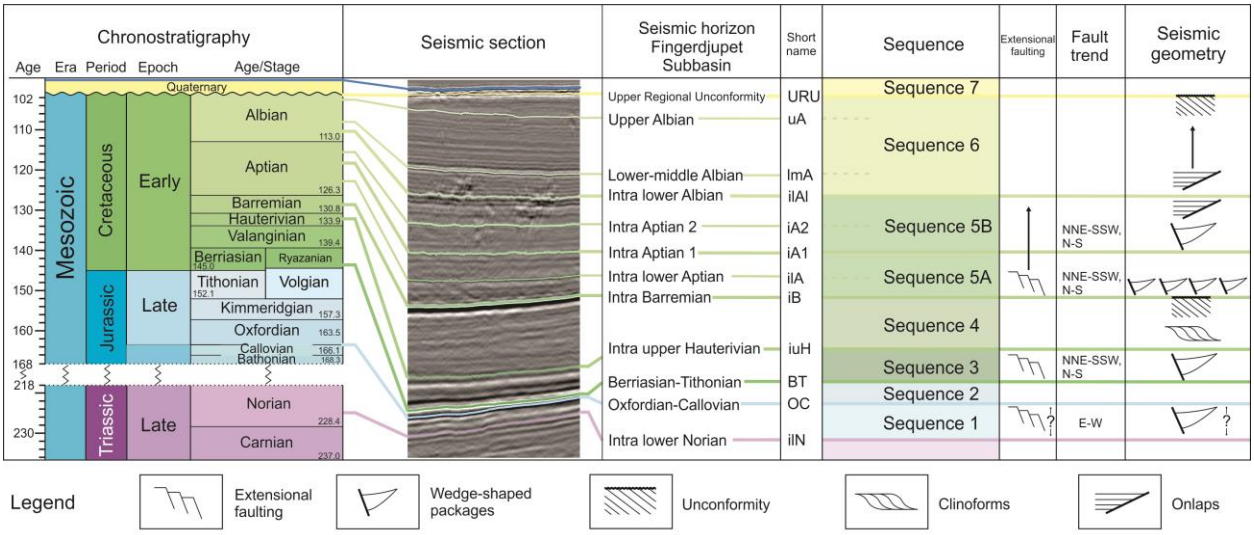

1075

1076 *Fig. 6:*

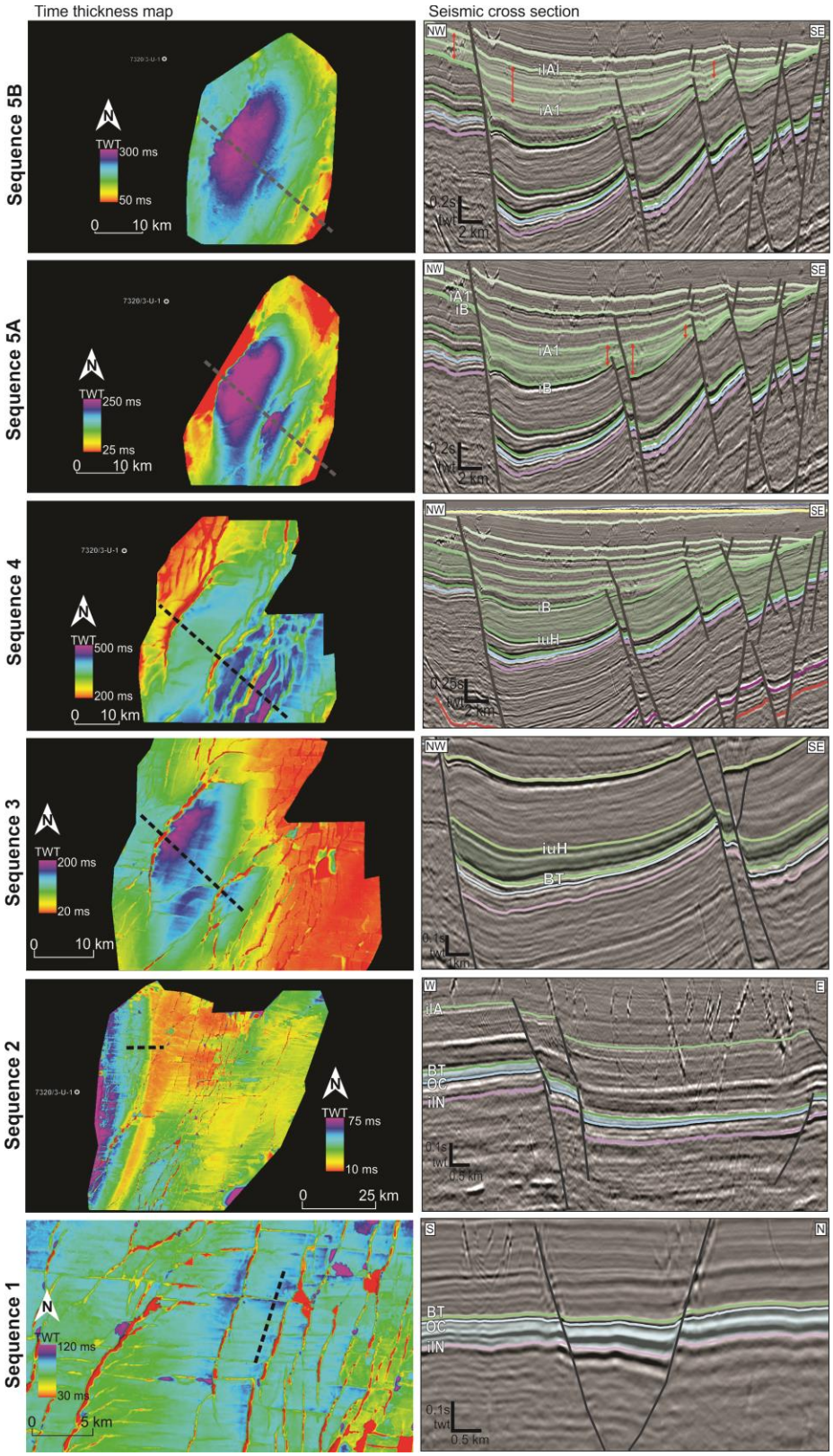

1077

1078 *Fig. 7:*

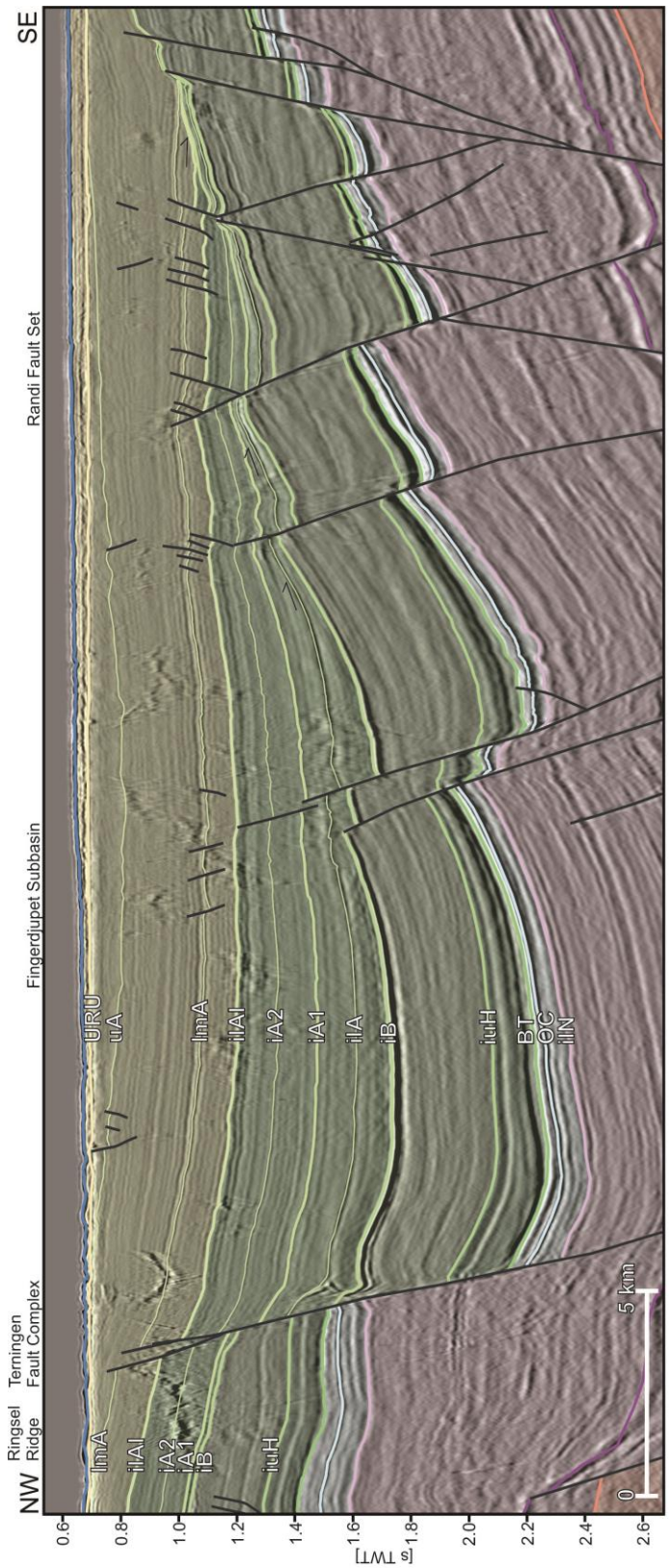

1079

1080 *Fig. 8:*

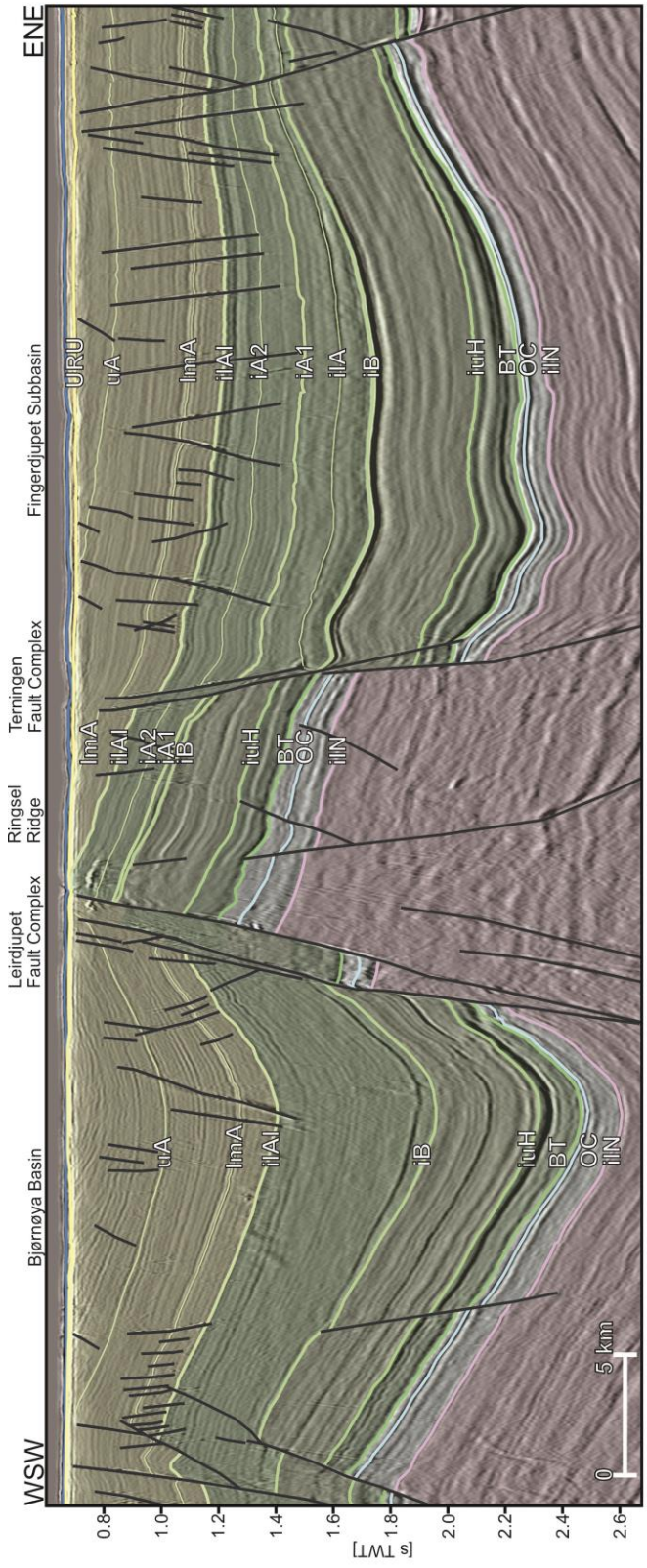

1081

Fig. 9:

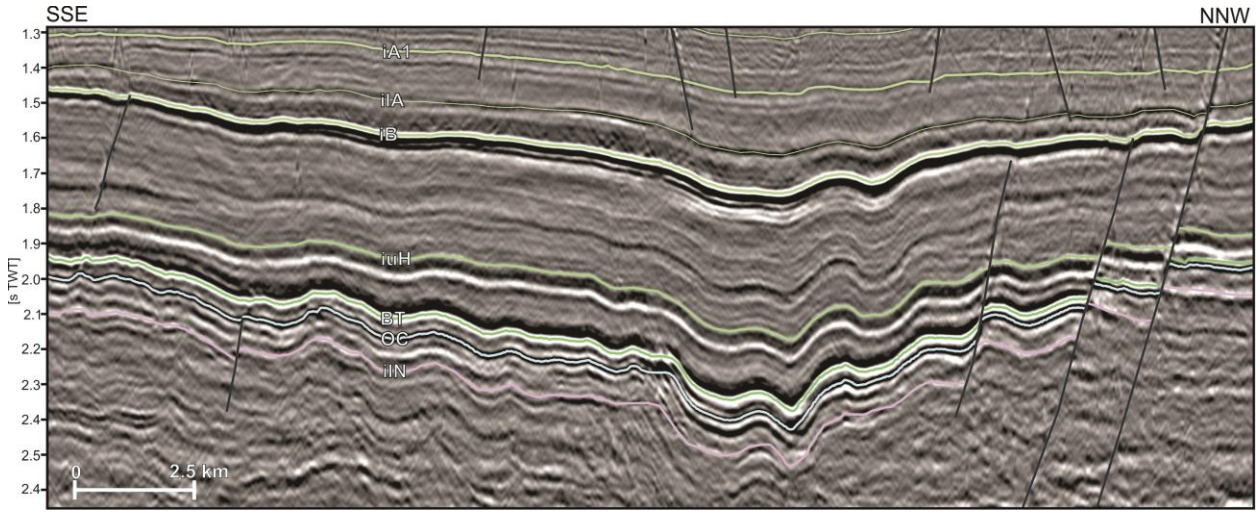
SSE
NNW
[s TWT]
1.3
1.4
1.5
1.6
1.7
1.8
1.9
2.0
2.1
2.2
2.3
2.4
2.5
2.4
iA1
iIA
iB
iuH
BT
OC
iN
0
2.5 km

1084 *Fig. 10:*

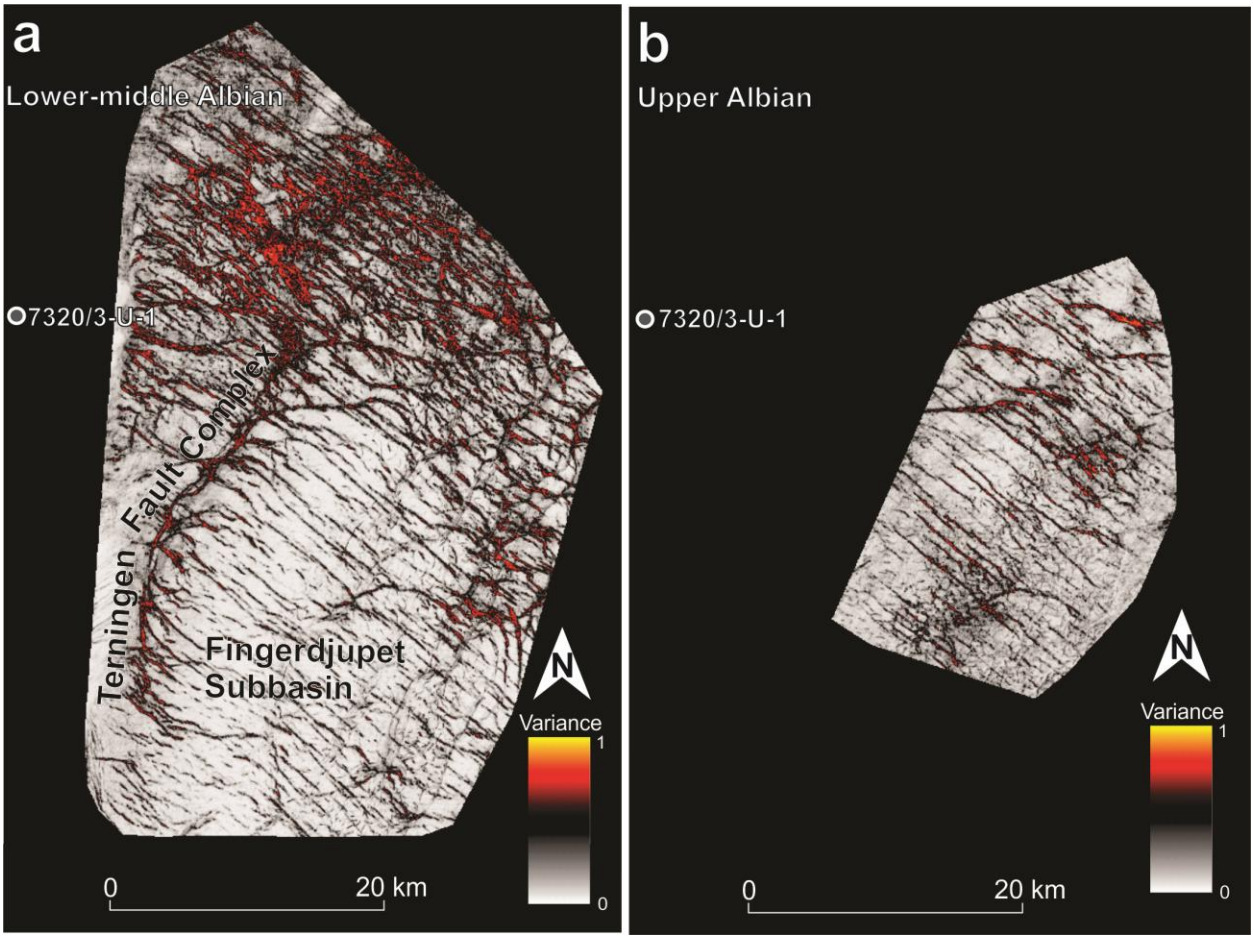

1085

1086 *Fig. 11:*

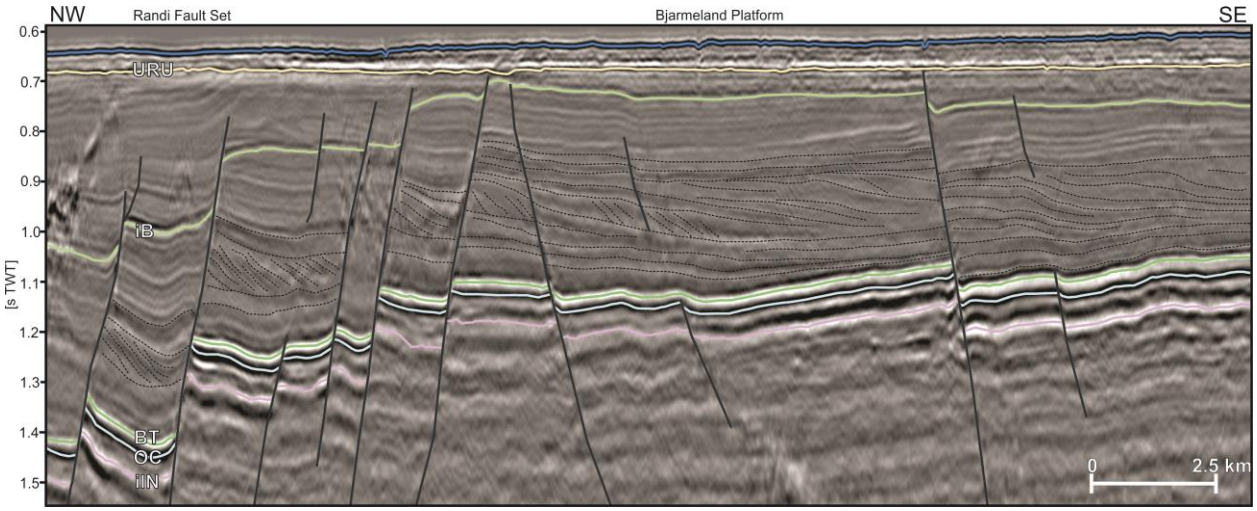

1087

Fig. 12:

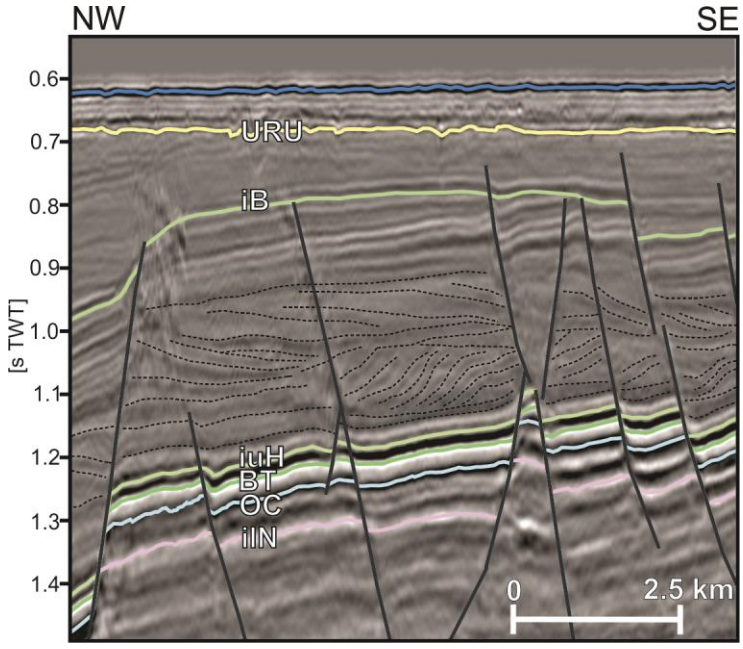

1090 *Fig. 13:*

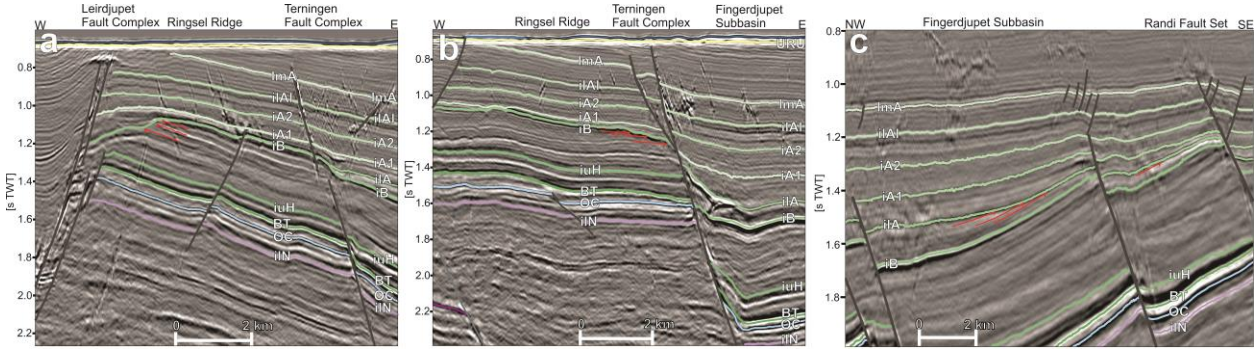

1091